Version of Record: https://www.sciencedirect.com/science/article/pii/S0003491621001871
Manuscript_502aa28076d5bc93034075540dd2d463

Geometry and entanglement in the scattering matrix

Silas R. Beane and Roland C. Farrell

InQubator for Quantum Simulation (IQuS), Department of Physics,
University of Washington, Seattle, WA 98195.

Abstract: A formulation of nucleon-nucleon scattering is developed in which the S-matrix, rather than an effective-field theory (EFT) action, is the fundamental object. Spacetime plays no role in this description: the S-matrix is a trajectory that moves between RG fixed points in a compact theory space defined by unitarity. This theory space has a natural operator definition, and a geometric embedding of the unitarity constraints in four-dimensional Euclidean space yields a flat torus, which serves as the stage on which the S-matrix propagates. Trajectories with vanishing entanglement are special geodesics between RG fixed points on the flat torus, while entanglement is driven by an external potential. The system of equations describing S-matrix trajectories is in general complicated, however the very-low-energy S-matrix —that appears at leading-order in the EFT description— possesses a UV/IR conformal invariance which renders the system of equations integrable, and completely determines the potential. In this geometric viewpoint, inelasticity is in correspondence with the radius of a three-dimensional hyperbolic space whose two-dimensional boundary is the flat torus. This space has a singularity at vanishing radius, corresponding to maximal violation of unitarity. The trajectory on the flat torus boundary can be explicitly constructed from a bulk trajectory with a quantifiable error, providing a simple example of a holographic quantum error correcting code.

NT@UW-20-08, IQuS@UW-20-01

© 2021 published by Elsevier. This manuscript is made available under the Elsevier user license
https://www.elsevier.com/open-access/userlicense/1.0/

Contents

1 Introduction **2**

2 S-matrix and spin entanglement **5**
- 2.1 Phase shifts, fixed points and momentum flow 5
- 2.2 Entanglement power defined 10
- 2.3 Effective range theory at leading order 12
- 2.4 Conformal range model 16

3 Geometry of the S-matrix **18**
- 3.1 Hilbert-Schmidt Distance 18
- 3.2 Entanglement power as a distance measure 19
- 3.3 Embedding in $\mathbb{R}^4$ 20
- 3.4 Flat torus isometry group 21

4 S-matrix theory of scattering **21**
- 4.1 Action principle 21
- 4.2 Geodesics on the flat torus 22
- 4.3 Entanglement forces and the ERE 22

5 Inelasticity and holography **28**
- 5.1 Inelasticity and the bulk 28
- 5.2 Embedding in $\mathbb{R}^4$ 29
- 5.3 Geodesics in the bulk 30
- 5.4 Recovery of the ERE and error correction 32

6 Projections on $\mathbb{R}^2$ and $\mathbb{R}^3$ **34**
- 6.1 Non-conservative entanglement forces 34
- 6.2 Embedding in $\mathbb{R}^2$ 35
- 6.3 Quartics and the squere 36
- 6.4 Embedding in $\mathbb{R}^3$ 37

7 Summary and discussion **38**

1 Introduction

In a generic quantum-mechanical scattering process, it is usual to view an effective field theory (EFT) action as the fundamental object from which all information about the scattering process can be obtained. General physical principles as well as the internal and spacetime symmetries of the system in question are conveniently encoded in the EFT [1], which is given a precise definition as a perturbative expansion in local operators about a fixed point of the renormalization group (RG) [2]. This view of scattering is remarkably successful and intuitive. As scattering processes take place in spacetime and the fundamental experimental knobs are momentum and energy, it stands to reason that the suitable stage for describing the process is spacetime itself. On the other hand, there are many things going on in the scattering process which a description based on local interactions in spacetime may not capture. For instance, the system could be highly entangled in all its degrees of freedom, and quantum entanglement is intrinsically non-local in spacetime. This raises the question of whether important effects may be missing in field-theoretic descriptions of physical systems where entanglement is expected to play a role. Recent work, based on earlier work in Refs. [3–5], has investigated this issue in free scalar field theory in $1+1$ dimensions and found evidence for an exponential suppression of quantum correlations which can lead to the presence of a new relative length scale associated with geometric entanglement [6].

Abandoning a description in terms of local operators suggests abandoning spacetime as the stage on which the scattering is defined and described.[1] What then is the appropriate stage on which to describe the scattering process which renders the quantum-entangling properties manifest? This is the main question addressed in this paper. Consider abandoning locality in spacetime and focusing on a more fundamental principle: unitarity. This in turn suggests that the unitary S-matrix replace the action as the fundamental object which characterizes the scattering process. If spacetime is the stage on which EFT interactions are defined, what is the stage on which the unitary S-matrix propagates? In this paper, it is shown that the S-matrix is naturally viewed as a trajectory in a theory space that is defined by all possible unitary trajectories. A rather surprising and essential observation is that in special —yet relevant— cases, the S-matrix possesses symmetry that is not visible in the EFT description. In particular, in these cases, the S-matrix possesses a UV/IR conformal invariance which plays a critical role in all that follows.

While the considerations in this paper are quite general, the focus will be on the paradigmatic problem of s-wave nucleon-nucleon scattering. This system is ideal for addressing these questions as it constitutes the simplest kind of quantum-mechanical scattering with a finite-range potential, it has non-trivial spin and isospin and interesting properties as regards entanglement. Moreover the system exhibits a non-trivial fixed-point structure which defines the EFT of nucleon-nucleon scattering to be a perturbative expansion about a fixed point of the RG [10–13]. The EFT in question is, in some sense, the simplest low-energy EFT of the

[1] For recent efforts in formulating a spacetime-independent theory of perturbative gauge theory scattering amplitudes, see Refs. [7–9].

Standard Model. At momentum transfers small as compared to the mass of the pion, the leading-order (LO) effective Lagrangian, constrained by spin, isospin and Galilean invariance, can be put in the form[14]

$$\mathcal{L}_{\rm LO} = -\frac{1}{2}C_S(N^\dagger N)^2 - \frac{1}{2}C_T\left(N^\dagger\hat{\boldsymbol{\sigma}}N\right)\cdot\left(N^\dagger\hat{\boldsymbol{\sigma}}N\right) \ , \tag{1.1}$$

where N represents both spin states of the proton and neutron fields and $\hat{\boldsymbol{\sigma}}^\alpha$ are the Pauli spin matrices. These interactions can be re-expressed as contact interactions in the ${}^1S_0$ and ${}^3S_1$ channels with couplings $C_0 = (C_S - 3C_T)$ and $C_1 = (C_S + C_T)$ respectively, where the two couplings are fit to reproduce the ${}^1S_0$ and ${}^3S_1$ scattering lengths. Higher-order operators involve derivatives acting on the nucleon fields and give rise to effective range and shape-parameter corrections. The interactions of Eq. (1.1) are highly singular. Defining the couplings in dimensional regularization with the PDS scheme [10, 11], and choosing the renormalization scale to be the pion mass, one finds $C_T^{\rm PDS}/C_S^{\rm PDS} = 0.0824$. This well-known suppression of the spin-entangling operator that appears at LO in the EFT expansion has motivated the study of entanglement in (hyper)nuclear systems [15], as a measure of the degree of entanglement of interaction operators in the EFT would appear to be required.

Forget now about the EFT description and consider a direct construction of the nucleon-nucleon S-matrix. At low energies, neutrons and protons, with two spin degrees of freedom each, scatter via the phase shifts $\delta_{0,1}$, in the ${}^1S_0$ and ${}^3S_1$ channels, respectively, with projections onto higher angular momentum states suppressed by powers of the nucleon momenta. Neglecting the small tensor-force-induced mixing of the ${}^3S_1$ channel with the ${}^3D_1$ channel, the S-matrix for nucleon-nucleon scattering below inelastic threshold can be decomposed as

$$\hat{\mathbf{S}}(p) = \frac{1}{4}\left(3e^{i2\delta_1(p)} + e^{i2\delta_0(p)}\right)\hat{\mathbf{1}} \ + \ \frac{1}{4}\left(e^{i2\delta_1(p)} - e^{i2\delta_0(p)}\right)\hat{\boldsymbol{\sigma}}\cdot\hat{\boldsymbol{\sigma}} \ , \tag{1.2}$$

where in the direct-product space of the nucleon spins,

$$\hat{\mathbf{1}} \equiv \hat{\mathcal{I}}_2 \otimes \hat{\mathcal{I}}_2 \quad , \quad \hat{\boldsymbol{\sigma}}\cdot\hat{\boldsymbol{\sigma}} \equiv \sum_{\alpha=1}^{3} \hat{\boldsymbol{\sigma}}^\alpha \otimes \hat{\boldsymbol{\sigma}}^\alpha \ , \tag{1.3}$$

with $\mathcal{I}_2$ the 2×2 unit matrix. It is important to stress that this decomposition of the S-matrix follows from unitarity, the symmetries of the system, and from the fact that the nucleons are fermions. The standard procedure for obtaining the phase shifts is to compute the scattering amplitude using the EFT and then match onto the S-matrix. In this paper, a new method will be developed for obtaining the phase shifts, which does not rely on a spacetime picture involving local operators. Several issues immediately present themselves and will be discussed in turn.

First, the S-matrix in Eq. (1.2) is expressed as a function of the momentum variable p (which we take throughout as the center-of-mass momentum). The momentum variable arises naturally in the spacetime picture and the dependence of the phase shifts on momentum is determined by the expansion in local operators which is constrained by Galilean invariance.

In a spacetime-independent description of scattering, the choice of the momentum as the relevant variable is necessarily arbitrary, and indeed it will turn out that the choice of variable is related to the choice of parameterization of trajectories on a Riemannian manifold.

A second issue is that of the fixed-point structure of the EFT and how that manifests itself at the level of the S-matrix. In non-relativistic EFT, scale invariance at a fixed point is realized as Schrödinger symmetry of the EFT action.[2] Aside from the free theory, which clearly admits Schrödinger symmetry, non-relativistic EFT admits a non-trivial fixed point at the strongest possible coupling consistent with unitarity (known as "unitarity"). In the language of the effective range expansion (ERE), this corresponds to taking the s-wave scattering length to infinity while higher-order effective range and shape parameters are taken to zero. As the relation between the scattering length and the EFT operator couplings is renormalization scheme dependent, the EFT couplings in themselves carry no physical, scheme-independent, information; indeed in a mass-independent scheme the couplings are driven to infinity at unitarity, whereas in a mass-dependent scheme (like the PDS scheme) the couplings can be made to approach a number of order unity in units of the characteristic physical length scales. By contrast, as will be seen in detail below, the S-matrix provides a physical regularization of the infinite coupling limit as the fixed points arise at finite values of the S-matrix. The notion of RG flow in the EFT couplings will translate to S-matrix momentum flow, which will be described by equations that exhibit the fixed point structure of the RG.

A third issue regards measures of quantum entanglement. A common measure of the quantum entanglement in the EFT is the state-dependent entanglement entropy, which is generally highly singular in quantum field theory, much like the renormalized couplings. One may worry that by working directly with the S-matrix, one loses valuable information regarding the nature of the entangling properties of the interaction. However, a physical measure of the entanglement of interaction –the entanglement power (EP)– has recently been developed and applied to the unitary S-matrix.[3] The EP [20, 21] is a state-independent and physical measure of the entanglement induced by interaction, for instance by particular operators in an EFT. The EP of the nucleon-nucleon S-matrix was recently considered in Ref. [15].

Tying these last two issues together, this paper will show that the fixed-point structure of the S-matrix has geometrical significance whose origin is closely tied with quantum entanglement. In particular, one may view the RG fixed points as vertices on a compact two-dimensional surface, with the S-matrix a trajectory that moves on this manifold between the fixed points. In the absence of EP the surface appears as a lattice of fixed points; the S-matrix is constrained to one dimensional motion along a geodesic, providing links between the RG fixed points. Only in the presence of entanglement does the surface appear as a flat torus, a flat, compact Riemannian manifold.

In one of the more striking consequences of the geometric formulation of scattering, inelasticity –a non-local effect in the effective field theory— is, in its simplest realization, in cor-

[2] For the present context, see Refs. [16–18].

[3] For previous work on the entanglement generated in non-relativistic scattering see Ref. [19].

respondence with the radius of a three-dimensional hyperbolic space whose two-dimensional boundary is the flat torus. This space has a singularity at vanishing radius, corresponding to maximal violation of unitarity. The boundary geodesic can be explicitly constructed from a bulk geodesic with a quantifiable error, providing a simple example of holographic duality and quantum error correction.

This paper is organized as follows. Section 2 sets up the S-matrix framework. First, some essential properties of the S-matrix are introduced in the context of single-channel s-wave scattering. Then various analogous properties of the nucleon-nucleon S-matrix are considered, including the fixed points of the RG, the parameterization of the S-matrix, the EP and the momentum flow. This is followed by the consideration of the two specific S-matrices that will be treated. The main example that will be focused on is LO in the ERE which corresponds to the scattering length approximation (LO in the EFT). A second example, the conformal range model, includes effective range corrections but in a manner that is correlated between the two channels to maintain a UV/IR conformal symmetry. Section 3 develops the geometric picture of the S-matrix. First, a coordinate-independent operator-defined metric is introduced using the notion of the Hilbert-Schmidt distance between operators. This is followed by construction of the embedding of the S-matrix unitarity constraints in the four-dimensional Euclidean space $\mathbb{R}^4$. This embedding gives rise to the flat torus which is the two-dimensional manifold on which the S-matrix propagates. The isometries of the flat torus are then considered in detail. Section 4 is in some sense the main section of the paper. First, the general action principle which describes the S-matrix trajectories is considered. In turn, the geodesics on the flat torus are constructed, followed by a recovery of LO in the ERE by positing an external entangling potential. The conformal range model is also analyzed and its potential is found. Section 5 relaxes the unitarity condition to consider inelastic loss. The geodesics on the resulting hyperbolic geometry are constructed, and, in the presence of a modified external potential, LO in the ERE is recovered up to a quantifiable error. In Section 6, the geometry of the projections of the flat torus on two- and three-dimensional spaces is considered, and it is explicitly shown how non-conservative forces are necessary to describe trajectories on the projected spaces. Finally, Section 7 is a summary of the geometrical S-matrix construction and a discussion of open questions and future work.

2 S-matrix and spin entanglement

2.1 Phase shifts, fixed points and momentum flow

Single-channel scattering

In single-channel, non-relativistic, s-wave scattering below inelastic threshold, the S-matrix in manifestly unitary form can be expressed as

$$S(p) = e^{i2\delta(p)} = \frac{1 + i\tan\delta(p)}{1 - i\tan\delta(p)} , \tag{2.1}$$

where $\delta(p)$ is the phase shift and p is the center-of-mass momentum. The (scale-invariant) RG fixed points of the S-matrix occur when there is no interaction, $\tan\delta(p) = 0$ ($\delta = 0$), or when the interaction is maximal, $\tan\delta(p) = \infty$ ($\delta = \frac{\pi}{2}$), corresponding to $S(p) = 1$ or -1, respectively. The assumption that $p\cot\delta(p)$ is analytic in p^2 is sufficient to give the ERE, where at LO in the ERE, $\tan\delta(p) = -pa + \mathcal{O}(p^3)$, with a the scattering length. In the limit that $a \to 0$ ($\pm\infty$) while effective range and shape parameters are taken to zero, $S(p) \to 1$ (-1). Parameterizing the S-matrix as $S = x + iy$ constrains the S-matrix to the unit circle in the x-y plane as shown in Fig. (1).

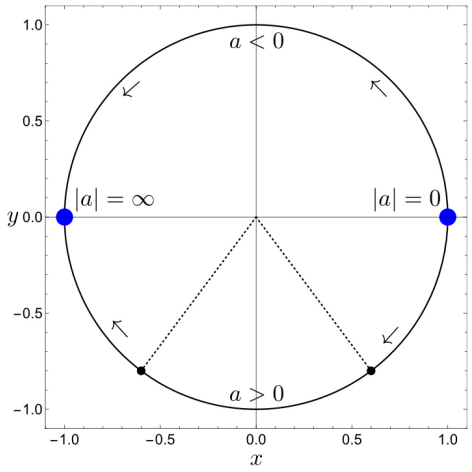

Figure 1. The unitarity unit circle for single-channel scattering. In these coordinates, the S-matrix is a trajectory from the trivial fixed point (blue dot on the right) to the non-trivial fixed point (blue dot on the left). At LO in the ERE, there is a conformal transformation on the momenta which takes the phase shift to minus itself modulo $\pi/2$. The two black dots are related by a conformal transformation. The upper (lower) half-circle corresponds to negative (positive) scattering length.

Consider LO in the ERE and assume that all inelastic thresholds are pushed to infinity so that p is defined on the interval $[0, \infty)$. The real coordinates are

$$x(p) = \frac{1 - a^2p^2}{1 + a^2p^2} \quad , \quad y(p) \; = \; -\frac{2ap}{1 + a^2p^2} \; . \tag{2.2}$$

Note that a rescaling of the momenta is compensated by a rescaling of the scattering length; i.e. x and y are invariant with respect to the dilatation $p \mapsto e^{\epsilon}p$, $a \mapsto e^{-\epsilon}a$. This scale invariance implies that the fixed points of the RG are accessed by varying the scattering lengths at fixed momenta or varying the momenta at fixed scattering length. Hence, under the action of a momentum dilatation $p \mapsto e^{\epsilon}p$, for small ϵ, the S-matrix beta-function can be defined:

$$\beta(S) \equiv p\frac{d}{dp}S(p) \; = \; \frac{1}{\epsilon}\left(S(e^{\epsilon}p) - S(p)\right) \; , \tag{2.3}$$

where $\beta(S)$ depends on details of the dynamics and vanishes at the fixed points where $S^2 = 1$. At LO in the ERE, the S-matrix momentum flow is governed by

$$p\frac{d}{dp}S(p) = \tfrac{1}{2}\left(S^2 - 1\right) \ . \tag{2.4}$$

For a finite and fixed, the S-matrix trajectory begins at the trivial fixed point, $(x, y) = (1, 0)$ at $p = 0$, and flows to the non-trivial fixed point at $(-1, 0)$ when $p \to \infty$. This behavior of moving along a semi-circle holds for the full phase shift $\delta(p)$ as unitarity constrains the S-matrix to one dimension and therefore there is no freedom to move off the unit circle in the absence of inelastic effects. Importantly, LO in the ERE has a special property beyond the scale transformation discussed above. Under the momentum inversion,

$$p \mapsto \frac{1}{a^2 p} \ , \tag{2.5}$$

the coordinates transform as $(x, y) \to (-x, y)$ and the phase shift transforms as $\delta(p) \to -\delta(p) \pm \pi/2$. This symmetry will be referred to as a conformal transformation as it leaves the phase shift invariant modulo fixed phases. However, note that this is a symmetry transformation that interchanges the UV and the IR. As such, this symmetry is generally broken by higher orders in the ERE. The conformal invariance is not particularly illuminating in single-channel scattering as unitarity constrains the one-dimensional S-matrix trajectory to move in a one-dimensional space. However, in systems where unitarity constrains the S-matrix to a surface with dimension greater than one, the conformal invariance will be seen to provide a powerful constraint.

Nucleon-nucleon scattering: coordinates and fixed points

The fixed points of the nucleon-nucleon S-matrix occur when the phase shifts both vanish, $\delta_1 = \delta_0 = 0$, or are both at unitarity, $\delta_1 = \delta_0 = \frac{\pi}{2}$, or when $\delta_1 = 0$, $\delta_0 = \frac{\pi}{2}$ or $\delta_1 = \frac{\pi}{2}$, $\delta_0 = 0$. The S-matrices at these fixed points are the general solution of the equation $\hat{\mathbf{S}}^2 = \hat{\mathbf{1}}$ and are given by

$$\begin{aligned} \hat{\mathbf{S}}_{①} = +\hat{\mathbf{1}} \quad &, \quad \hat{\mathbf{S}}_{③} \ = \ +(\hat{\mathbf{1}} + \hat{\boldsymbol{\sigma}} \cdot \hat{\boldsymbol{\sigma}})/2 \ , \\ \hat{\mathbf{S}}_{②} = -\hat{\mathbf{1}} \quad &, \quad \hat{\mathbf{S}}_{④} \ = \ -(\hat{\mathbf{1}} + \hat{\boldsymbol{\sigma}} \cdot \hat{\boldsymbol{\sigma}})/2 \ . \end{aligned} \tag{2.6}$$

These fixed points furnish a representation of the Klein four-group, $\mathbb{Z}_2 \otimes \mathbb{Z}_2$. As this is the discrete symmetry group of the rhombus, the fixed points, which by construction provide the boundaries of unitary interactions, suggest a geometrical interpretation of the S-matrix as a trajectory within a rhombus whose vertices are the fixed points of the RG and mark the most extreme values that the S-matrix can achieve consistent with unitarity.

It is straightforward to make this geometrical construction precise. In a $\mathbb{Z}_2$ basis consisting of $\hat{\mathbf{1}}$ and $(\hat{\mathbf{1}} + \hat{\boldsymbol{\sigma}} \cdot \hat{\boldsymbol{\sigma}})/2$, the S-matrix can be decomposed as

$$\hat{\mathbf{S}} = \frac{1}{2}\left(e^{i2\delta_1} + e^{i2\delta_0}\right)\hat{\mathbf{1}} \ + \ \frac{1}{2}\left(e^{i2\delta_1} - e^{i2\delta_0}\right)\left(\hat{\mathbf{1}} + \hat{\boldsymbol{\sigma}} \cdot \hat{\boldsymbol{\sigma}}\right)/2 \ . \tag{2.7}$$

It is convenient to adopt the coordinates

$$\hat{\mathbf{S}} = u(p)\,\hat{\mathbf{1}} \;+\; v(p)\;\left(\hat{\mathbf{1}} + \hat{\boldsymbol{\sigma}}\cdot\hat{\boldsymbol{\sigma}}\right)/2\;, \tag{2.8}$$

where $u(p)$ and $v(p)$ are complex functions decomposed in terms of real functions as

$$u(p) \;=\; x(p) \;+\; i\,y(p) \quad , \quad v(p) \;=\; z(p) \;+\; i\,w(p)\;. \tag{2.9}$$

Unitarity provides two constraints on the four parameters; the first constraint defines the unit three-sphere S^3:

$$\bar{u}u \;+\; \bar{v}v \;=\; 1 \;=\; x^2 \;+\; y^2 \;+\; z^2 \;+\; w^2\;, \tag{2.10}$$

and the second constraint,

$$\bar{u}v + \bar{v}u \;=\; 0 \;=\; xz \;+\; yw\;, \tag{2.11}$$

is a projective constraint whose intersection with S^3 provides the manifold on which the S-matrix trajectory propagates. This choice of coordinates is by no means unique. A general parameterization of the S-matrix is

$$\hat{\mathbf{S}} = \left[x(p) \;+\; i\,y(p)\right]\hat{\mathbf{1}} \;+\; \left[z(p) \;+\; i\,w(p)\right]\left(\hat{\mathbf{1}}\beta + \hat{\boldsymbol{\sigma}}\cdot\hat{\boldsymbol{\sigma}}\alpha\right)\;. \tag{2.12}$$

With the coordinate choice

$$\begin{aligned} x &= \tfrac{1}{4\alpha}[(3\alpha-\beta)\cos(\theta) + (\alpha+\beta)\cos(\phi)]\;, \\ y &= \tfrac{1}{4\alpha}[(3\alpha-\beta)\sin(\theta) + (\alpha+\beta)\sin(\phi)]\;, \\ z &= \tfrac{1}{4\alpha}[-\cos(\phi)+\cos(\theta)]\;, \\ w &= \tfrac{1}{4\alpha}[-\sin(\phi)+\sin(\theta)]\;, \end{aligned} \tag{2.13}$$

$\hat{\mathbf{S}}$ is independent of the parameters α and β. Here we have defined $\phi \equiv 2\delta_0$ and $\theta \equiv 2\delta_1$. The unitarity constraints now take the form

$$\begin{aligned} 1 \;&=\; (x + (\alpha+\beta)\,z)^2 \;+\; (y + (\alpha+\beta)\,w)^2\;, \\ (\alpha \;-\; \beta)\left(w^2 \;+\; z^2\right) \;&=\; xz \;+\; yw\;. \end{aligned} \tag{2.14}$$

Requiring that the coordinate system (x, y, z, w) describe an isotropic space yields the constraints $3\alpha - \beta = \alpha + \beta = 1$, or $\alpha = \beta = 1/2$ which recovers the choice made above in Eq. (2.8) and Eq. (2.9), and leads to the parameterization of the S-matrix that will be used throughout this paper[4]:

$$\begin{aligned} x \;&=\; \tfrac{1}{2}\,r[\cos(\phi)+\cos(\theta)] \quad , \quad y \;=\; \tfrac{1}{2}\,r[\sin(\phi)+\sin(\theta)]\;, \\ z \;&=\; \tfrac{1}{2}\,r[-\cos(\phi)+\cos(\theta)] \quad , \quad w \;=\; \tfrac{1}{2}\,r[-\sin(\phi)+\sin(\theta)]\;, \end{aligned} \tag{2.16}$$

[4] Another useful isotropic parameterization of the S-matrix is given by the Hopf-like coordinates,

$$\begin{aligned} x \;&=\; r\cos\xi\sin\eta \quad , \quad y \;=\; r\sin\xi\sin\eta\;, \\ z \;&=\; r\sin\xi\cos\eta \quad , \quad w \;=\; -r\cos\xi\cos\eta\;. \end{aligned} \tag{2.15}$$

with $\xi \in [0, 2\pi)$ and $\eta \in [0, \pi]$.

with $\phi \in [0, 2\pi]$ and $\theta \in [0, 2\pi]$ and $r = 1$. Note that the four coordinates span the range $[-1, 1]$.

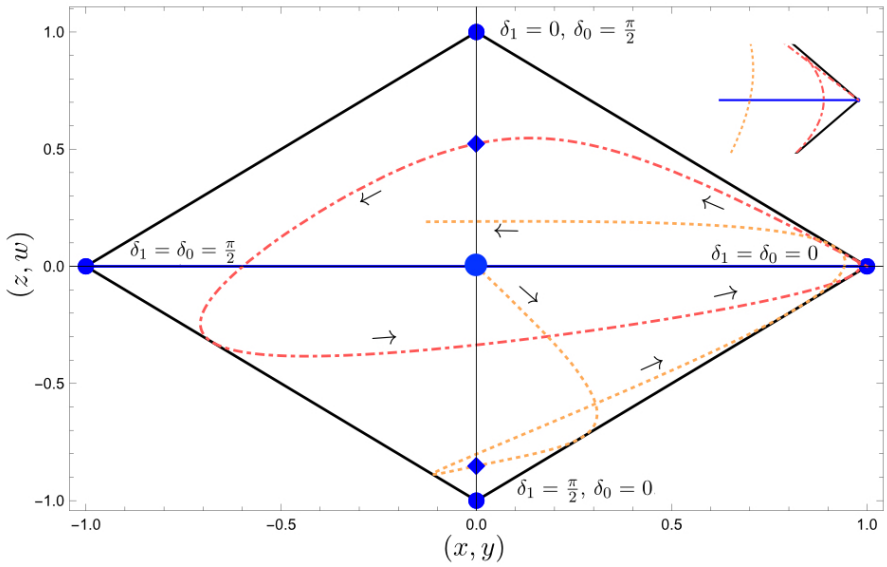

Figure 2. Rhombus in the $u - v$ plane with fixed points (blue dots) at the vertices. The dot-dashed red curve corresponds to the real part of $\hat{\mathbf{S}}$ in the $x-z$ plane, and the dashed orange curve corresponds to the imaginary part of $\hat{\mathbf{S}}$ in the $y-w$ plane. These trajectories are obtained from the Nijmegen phase shift analysis (PWA93) in Ref. [22] and plotted from $p = 0$ to 400 MeV with the arrows indicating the direction of momentum flow. The blue diamonds correspond to the point at which the phase shifts differ by $\pi/2$ and the EP vanishes. The inset is a magnification of the right corner.

The fixed points of the RG in (x, y, z, w) coordinates are:

$$\begin{aligned} \hat{\mathbf{S}}_{①} &= (+1,\ 0,\ 0,\ 0) \quad , \quad \hat{\mathbf{S}}_{③} = (\ 0,\ 0, +1,\ 0)\ , \\ \hat{\mathbf{S}}_{②} &= (-1,\ 0,\ 0,\ 0) \quad , \quad \hat{\mathbf{S}}_{④} = (\ 0,\ 0, -1,\ 0)\ . \end{aligned} \tag{2.17}$$

A geometrical description of scattering follows by mapping the $\mathbb{Z}_2$ basis to the $u-v$ plane[5] with u representing the $\hat{\mathbf{1}}$ axis and v representing the $(\hat{\mathbf{1}}+\hat{\boldsymbol{\sigma}}\cdot\hat{\boldsymbol{\sigma}})/2$ axis. The fixed points sit on the extrema of the axes in the $x-z$ plane. However, in the $y-w$ plane, the fixed points all sit at the origin. In the plane defined by these new coordinates, the real and imaginary parts of the S-matrix are confined to fall within the boundaries set by $x+z = \pm 1$ and $x-z = \pm 1$, and $y+w = \pm 1$ and $y-w = \pm 1$, respectively. These boundaries define a rhombus in the $u-v$ plane as shown in Fig. (2). The dihedral group D_2, which is the symmetry group of the rhombus, corresponds to the coordinate transformations $(u, v) \to (u, v)$ (identity), $(u, v) \to (-u, v)$ (reflection about v), $(u, v) \to (u, -v)$ (reflection about u), and $(u, v) \to (-u, -v)$ (rotation of axes by π). D_2 is isomorphic to the Klein four-group, $\mathbb{Z}_2 \otimes \mathbb{Z}_2$. From Eq. (2.7), it is clear that

[5] In what follows, the $u - v$ plane will refer collectively to the $x - z$ and $y - w$ planes for the real and imaginary parts of the S-matrix, respectively.

when $\delta_0(p) = \delta_1(p)$, the S-matrix is (trivially) symmetric with respect to the $\mathbb{Z}_2$ subgroup $(u, v) \to (u, v)$ and $(u, v) \to (u, -v)$ of the Klein group. The nucleon-nucleon S-matrix taken from scattering data in the form of the Nijmegen phase-shift analysis [22] is plotted in Fig. (2).

The projection of the (x, y, z, w) coordinates onto two dimensions allows a visualization of the real and imaginary parts of the S-matrix. However as noted above, in the $y - w$ plane the fixed points sit on top of each other whereas it is clear from Eq. (2.17) that the four fixed points are distinct points in the four dimensional space. Distinct locations of the fixed points is achieved by projecting instead onto three of the four dimensions[6]. However, what is desired is a geometrical description of the S-matrix which captures the four-dimensional nature of the space via the two independent degrees of freedom given by the phase shifts ϕ and θ.

2.2 Entanglement power defined

A direct consequence of the geometric picture of the S-matrix as a trajectory confined to a rhombus is that when $\delta_0(p) = \delta_1(p)$, the S-matrix trajectory is a line (geodesic) between fixed points of the RG and resides on a symmetry axis of the rhombus that is protected by a $\mathbb{Z}_2$ subgroup of the Klein four-group. In the EFT description this enhanced symmetry is Wigner's $SU(4)$ spin-flavor symmetry where the two spin states of the neutron and of the proton transform as the four-dimensional fundamental representation [23–25]. This symmetry also arises from the large-N_c expansion in QCD [26–28] and from the near Schrödinger symmetry of the system implied by the large value of the physical scattering lengths as compared to QCD length scales [16]. As this enhanced symmetry suggests a suppression of spin-entangling interactions, there is motivation to develop measures of entanglement that are suitable for classifying interactions.

In a recent paper [15], it was shown that the EP, a state-independent measure of quantum entanglement, can be defined for the S-matrix:

$$\mathcal{E}(\hat{\mathbf{S}}) = 1 - \int \frac{d\Omega_1}{4\pi} \frac{d\Omega_2}{4\pi} \, \mathrm{Tr}_1 \left[\, \hat{\rho}_1^2 \, \right] \mathcal{P}\left(\Omega_1, \Omega_2\right) \ , \tag{2.18}$$

where $\hat{\rho}_1 = \mathrm{Tr}_2 \left[\, \hat{\rho}_{12} \, \right]$ is the reduced density matrix of the two-particle density matrix $\hat{\rho}_{12} = |\psi_{\mathrm{out}}\rangle\langle\psi_{\mathrm{out}}|$ with $|\psi_{\mathrm{out}}\rangle = \hat{\mathbf{S}}|\psi_{\mathrm{in}}\rangle$, and $\mathcal{P}$ is a probability distribution. The EP can be motivated as follows. Consider the non-entangled 'in' state of the spin of two nucleons, $\Omega_1 \otimes \Omega_2$, where $\Omega_{1,2}$ correspond to points on the Bloch sphere. After scattering, the outgoing state is generically no longer a product state and thus exhibits some amount of entanglement. The entanglement is quantified by the exponential of the second Rényi entropy, $\mathrm{Tr}_1 \left[\, \hat{\rho}_1^2 \, \right]$. This non-unique entanglement measure is chosen as it is particularly simple to evaluate analytically. The final step is to sum the entanglement of the 'out' state for every possible 'in' state; this is the integration over the two Bloch spheres in Eq. (2.18). This ensures that the EP is a state independent measure of entanglement and thus solely a property of the

[6] The geometry of projections onto subspaces of the four-dimensional space will be considered in detail in the final section.

S-matrix. For nucleon-nucleon scattering, the EP of $\hat{\mathbf{S}}$ is

$$\mathcal{E}(\hat{\mathbf{S}}) = N_{\mathcal{P}} \, \sin^2\left(2(\delta_1 - \delta_0)\right) \ , \tag{2.19}$$

where $N_{\mathcal{P}}$ is a numerical prefactor[7]. Expressed in terms of the coordinates (u, v) and (x, y, z, w), one has

$$\mathcal{E}(\hat{\mathbf{S}}) = 4N_{\mathcal{P}} \, |u|^2|v|^2 \ = \ 4N_{\mathcal{P}} \, \left(x^2 + y^2\right)\left(z^2 + w^2\right) \ , \tag{2.20}$$

and it is clear that the EP has geometrical significance as a measure of length. (A concrete operator definition will be provided below.) The EP vanishes when $\delta_1(p) - \delta_0(p) = m\frac{\pi}{2}$ for any integer m. This includes the $\mathbb{Z}_2$ symmetric line $\delta_1(p) = \delta_0(p)$ as well as the one point at which the phase shifts differ by $\pi/2$ (the blue diamond in Fig. (2)). The EP is plotted for the Nijmegen phase shift analysis [22] in Fig. (3). In addition, the EP vanishes at the four fixed points of the renormalization group. In general, the EP vanishes when

$$\hat{\mathbf{S}} \ = \ e^{i2\delta_0}\hat{\mathbf{S}}_{①} \quad \text{or} \quad \hat{\mathbf{S}} \ = \ -e^{i2\delta_0}\hat{\mathbf{S}}_{③} \ . \tag{2.21}$$

Therefore, in the absence of EP, the S-matrix is characterized by two curves that connect the fixed points $\hat{\mathbf{S}}_{①}$ and $\hat{\mathbf{S}}_{②}$ and $\hat{\mathbf{S}}_{③}$ and $\hat{\mathbf{S}}_{④}$ via the flow of the single phase shift $\delta_0(p)$ from 0 to $\pi/2$.

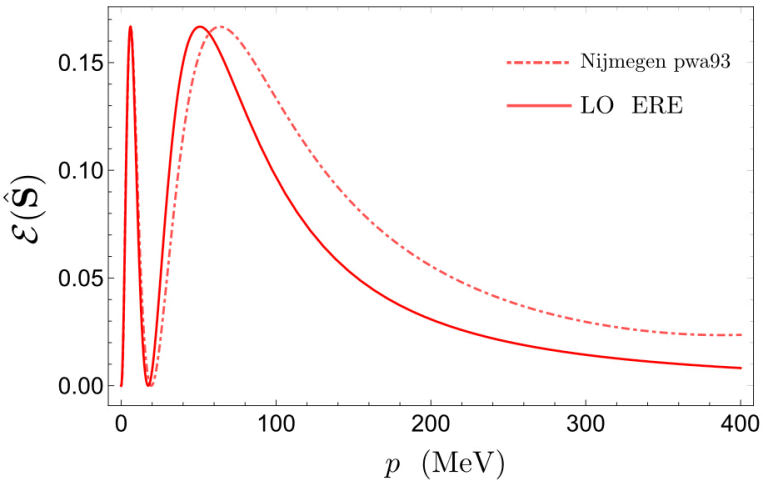

Figure 3. The EP obtained from Eq. (2.19) using the Nijmegen phase shift analysis in Ref. [22] (dot-dashed red curve), from Eq. (2.33) using the scattering length only (red curve).

Adapting momentum flow to the nucleon-nucleon system, consider the S-matrix under the action of a momentum dilatation $p \mapsto e^{\epsilon}p$. For small ϵ,

$$\hat{\beta}(\hat{\mathbf{S}}) \equiv p\frac{d}{dp}\hat{\mathbf{S}}(p) = \frac{1}{\epsilon}\left(\hat{\mathbf{S}}(e^{\epsilon}p) - \hat{\mathbf{S}}(p)\right) \ , \tag{2.22}$$

[7]With $\mathcal{P} = 1$, $N_{\mathcal{P}} = 1/6$. Choosing a distribution with more structure changes this prefactor.

and $\hat{\beta}(\hat{\mathbf{S}}) = 0$ at the four fixed points where $\hat{\mathbf{S}}^2 = \hat{\mathbf{1}}$. In the $\mathbb{Z}_2$ basis one then has

$$\hat{\beta}(\hat{\mathbf{S}}) = \beta_u(p)\,\hat{\mathbf{1}} \;+\; \beta_v(p)\left(\hat{\mathbf{1}} + \hat{\boldsymbol{\sigma}}\cdot\hat{\boldsymbol{\sigma}}\right)/2\;, \tag{2.23}$$

with

$$\beta_u(p) \equiv p\frac{d}{dp}u(p) \quad , \quad \beta_v(p) \equiv p\frac{d}{dp}v(p)\;. \tag{2.24}$$

Eq. (2.20) makes clear that the EP is related to the distance of the u and v coordinates from the origin. However, given that the EP has support only away from the fixed points, one might expect that when the momentum dependence of the S-matrix is specified, the EP will be directly related to $\beta_{u,v}(p)$. Indeed, generalizing the expression for uv given in Eq. (2.45) to a linear combination of β_u and β_v with complex coefficients, it is straightforward to find an expression for the EP in terms of the beta functions alone

$$\mathcal{E}(\hat{\mathbf{S}}) = \frac{N_{\mathcal{P}}}{4}\left|\frac{\beta_{\bar{v}}(p)\beta_u(p) - \beta_{\bar{u}}(p)\beta_v(p)}{\beta^2_{\bar{u}}(p) - \beta^2_{\bar{v}}(p)}\right|^2 . \tag{2.25}$$

The EP expressed in this form exhibits its connection to the RG; scattering at the RG fixed points does not entangle spins.

2.3 Effective range theory at leading order

At LO in the ERE, the S-matrix is completely determined by the scattering lengths and is expressed in the chosen coordinate basis as

$$u(p) = \frac{1}{2}\left(\frac{1-ia_1p}{1+ia_1p} + \frac{1-ia_0p}{1+ia_0p}\right) \quad , \quad v(p) \;=\; \frac{1}{2}\left(\frac{1-ia_1p}{1+ia_1p} - \frac{1-ia_0p}{1+ia_0p}\right)\;. \tag{2.26}$$

In terms of phase shifts,

$$\phi \;=\; -2\tan^{-1}(a_0p) \quad , \quad \theta \;=\; -2\tan^{-1}(a_1p)\;. \tag{2.27}$$

The fixed points of the RG are now at $a_1 = a_0 = 0$, $|a_1| = |a_0| = \infty$, and at $a_1 = 0\,,\ |a_0| = \infty$, and $|a_1| = \infty\,,\ a_0 = 0$. In nucleon-nucleon scattering, the scattering lengths are determined experimentally to be $a_0 = -23.714 \pm 0.013$ fm and $a_1 = 5.425 \pm 0.002$ fm. As seen in Fig. (4), Eq. (2.26) provides a good approximation to the physical nucleon-nucleon S-matrix for $p \leq 10$ MeV, and, of course, this corresponds to leading-order in the EFT description. Now assume that all inelastic thresholds are pushed to infinity so that p is defined on the interval $[0, \infty)$, and further assume that all range and shape parameters vanish. These assumptions extend the LO ERE to arbitrarily high momenta. In the EFT, this corresponds to a theory with only momentum-independent contact interactions between nucleons; i.e. all derivative interactions are assumed to vanish. By construction this model maps onto the correct physics in the IR and reveals interesting properties of the S-matrix when extended to the UV.

The real and imaginary parts of the S-matrix, described by x and z, and by y and w, respectively, are in correspondence with distinct trajectories in the $u - v$ plane that

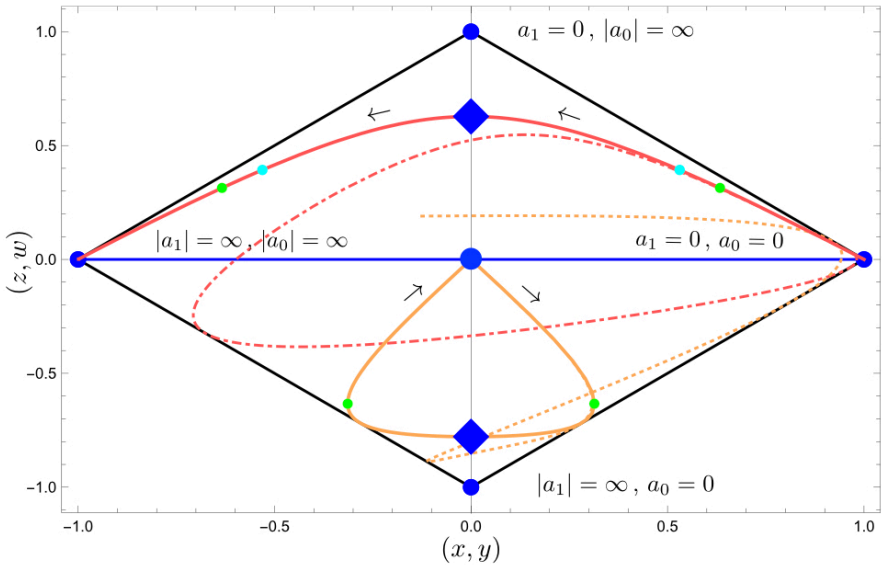

Figure 4. Rhombus in the $u - v$ plane with fixed points at the vertices and the origin. The solid red curve corresponds to the real part of $\hat{\mathbf{S}}$, and the solid orange curve corresponds to the imaginary part of $\hat{\mathbf{S}}$ at LO in the ERE, with the physical values of the nucleon-nucleon scattering lengths. The Nijmegen phase shift analysis [22] is also shown for comparison. The blue diamonds correspond to the fixed point of the UV/IR conformal transformation. The green dots are the maxima of the EP and the cyan dots are the maxima of a measure of curvature, as described in the text.

propagate between fixed points. A striking feature of Fig. (4) is the isometries of the S-matrix trajectories at LO in the ERE when the momenta ranges over the entire positive half line; for the physical scattering lengths, both the real and imaginary trajectories of S are $(u, v) \to (-u, v)$ symmetric. In order to analyze the isometries systematically, it is important to distinguish between the various cases which are determined by the relative signs of the scattering lengths. We will refer to the scenario where $a_1 a_0 < 0$ as "singly-bound" (one channel bound and the other unbound as in the physical case) and the scenario where $a_1 a_0 > 0$ as "doubly-(un)bound" (both channels bound or both channels unbound). The symmetry of the S-matrix and the EP are strikingly different in these two scenarios.

The isometries of the S-matrix trajectories are in correspondence with the UV/IR transformation on the momenta,

$$p \mapsto \frac{1}{|a_1 a_0| p} \ . \tag{2.28}$$

This invariance, generalized from single-channel scattering, is an intrinsic property of the LO ERE S-matrix at finite, non-zero values of the scattering lengths. That this symmetry is not visible in the LO EFT action is no surprise; the momentum range of the S-matrix has been extended to encompass the entire positive half line, and the symmetry interchanges the UV and the IR. Therefore, the S-matrix at LO in the ERE is a UV complete description

of scattering, in sharp contrast with the LO EFT description. The two fixed points of the conformal transformation are at $p = \pm\sqrt{|a_0 a_1|^{-1}}$. Therefore, for a given trajectory, only one of the fixed points of the transformation appears in the physical (scattering) region ($p \geq 0$) and lies on the axis of reflection of the corresponding isometry (the diamonds in Fig. (4)).

Acting with Eq. (2.28) on Eq. (2.26), it is straightforward to find the UV/IR transformation on the coordinates and angles:

$$\begin{aligned}
\underline{a_1 a_0 < 0}: \ & (x,z) \to (-x,z) \ , \ (y,w) \to (-y,w) \Longrightarrow \ (u,v) \to (-u,v) \ , \\
& (\phi,\theta) \to (\theta \mp \pi, \phi \pm \pi) \ , \\
\underline{a_1 a_0 > 0}: \ & (x,z) \to (-x,z) \ , \ (y,w) \to (y,-w) \Longrightarrow \ (u,v) \to (-\bar{u},\bar{v}) \ , \\
& (\phi,\theta) \to (-\theta \pm \pi, -\phi \pm \pi) \ .
\end{aligned} \tag{2.29}$$

Thus, the UV/IR transformation is a conformal transformation which leaves linear combinations of phase shifts invariant:

$$\begin{aligned}
\underline{a_1 a_0 < 0}: \ & \phi + \theta \to \phi + \theta \\
\underline{a_1 a_0 > 0}: \ & \phi - \theta \to \phi - \theta \ .
\end{aligned} \tag{2.30}$$

This conformal symmetry will prove critical in what follows.

For an illustration of the isometries in the $u - v$ plane with the scattering length magnitudes fixed to the physical case but with signs flipped, see Fig. (5).

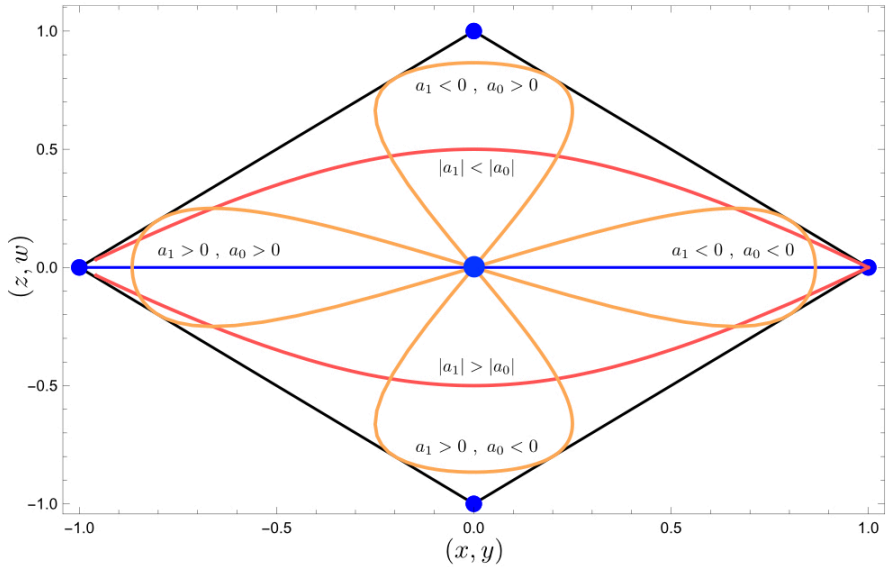

Figure 5. Rhombus in the $u - v$ plane with fixed points at the vertices and the origin. The solid red curves corresponds to the real part of $\hat{\mathbf{S}}$, and the solid orange curves corresponds to the imaginary part of $\hat{\mathbf{S}}$ at LO in the ERE. S-matrix trajectories with scattering lengths whose magnitudes are fixed to the physical values are displayed with all relative sign combinations.

At LO in the ERE, the beta functions for the coordinates are easily found to be

$$p\frac{d}{dp}v(p) = u(p)v(p) \quad , \quad p\frac{d}{dp}u(p) \;=\; \tfrac{1}{2}\left(u(p)^2 + v(p)^2 - 1\right) \;. \tag{2.31}$$

And consequently the momentum-flow equation for the S-matrix is

$$p\frac{d}{dp}\hat{\mathbf{S}} = \tfrac{1}{2}\left(\hat{\mathbf{S}}^2 \;-\; \hat{\mathbf{1}}\right) \;. \tag{2.32}$$

As in the single-channel case, this takes the form of the Ward identity for dilatations and therefore vanishes at the fixed points of the RG, as required. The content of this equation for phase shift degrees of freedom is a pair of decoupled, first-order, differential equations of the simple form $p\,\dot{\phi} = \sin\phi$ and $p\,\dot{\theta} = \sin\theta$ which immediately integrate to the solution of Eq. (2.27).

The EP of $\hat{\mathbf{S}}$ in terms of scattering lengths is

$$\mathcal{E}(\hat{\mathbf{S}}) = 4N_{\mathcal{P}}\frac{p^2\left(a_0 - a_1\right)^2\left(1 + a_1a_0p^2\right)^2}{\left(1 + a_0^2p^2\right)^2\left(1 + a_1^2p^2\right)^2} \;. \tag{2.33}$$

Note that there is a zero of the EP only in the singly-bound case. The EP is conformally invariant and has three (non-trivial) extrema as is evident in Fig. (3) in the physical case; there is a minimum at the conformal fixed point and two local maxima (shown as green dots on the S-matrix trajectory in Fig. (4)). The EP therefore behaves like the curvature of the S-matrix trajectory in the interior of the rhombus. A conformally invariant measure of curvature can be constructed from the square of the $z(p)$ coordinate beta function. This shares the bulk features of the EP in the singly-bound case, as shown in Fig. (3) (cyan dots), where $N_{\mathcal{P}}$ has been adjusted so that the maxima overlap. The EP must depend also on the imaginary trajectory as this contains information about the signs of the scattering lengths. Indeed, one readily finds that at LO in the ERE,

$$\mathcal{E}(\hat{\mathbf{S}}) = 4N_{\mathcal{P}}\big|\;\beta_v(p)\;\big|^2 \;. \tag{2.34}$$

Writing

$$\mathcal{E}(\hat{\mathbf{S}}) = \mathcal{E}(\mathrm{Re}\hat{\mathbf{S}}) \;+\; \mathcal{E}(\mathrm{Im}\hat{\mathbf{S}}) \;, \tag{2.35}$$

with

$$\mathcal{E}(\mathrm{Re}\hat{\mathbf{S}}) \;=\; N_{\mathcal{P}}\left(p\frac{d}{dp}z(p)\right)^2 \quad , \quad \mathcal{E}(\mathrm{Im}\hat{\mathbf{S}}) \;=\; N_{\mathcal{P}}\left(p\frac{d}{dp}w(p)\right)^2 \;, \tag{2.36}$$

one sees that there is a distinct contribution to the EP from each of the trajectories, both of which are related to the curvature of the $v(p)$ coordinate.

2.4 Conformal range model

Generally, the conformal invariance which interchanges the UV and the IR will be broken beyond LO in the ERE. Higher orders in the ERE include more short-distance structure, and maintaining a UV/IR symmetry will require contrivance[8]. Nevertheless, it is straightforward to find S-matrix models that include higher orders in the ERE and which possess UV/IR symmetry. These models are interesting as the stronger momentum dependence implies S-matrix trajectories with more complex curvature and EP. Consider

$$u(p) = \frac{1}{2}\left(\frac{1-ia_1(p)p}{1+ia_1(p)p} + \frac{1-ia_0(p)p}{1+ia_0(p)p}\right) \ , \ v(p) = \frac{1}{2}\left(\frac{1-ia_1(p)p}{1+ia_1(p)p} - \frac{1-ia_0(p)p}{1+ia_0(p)p}\right) , \quad (2.37)$$

where the momentum-dependent scattering length is defined as

$$a_r(p) = \frac{a_r}{1-\lambda a_r^2 p^2} \ , \quad (2.38)$$

and $\lambda > 0$ is a real number. This model reduces to the LO ERE when $\lambda = 0$, and with $\lambda \neq 0$ includes effective range corrections[9]. As in the LO ERE, the real and imaginary parts of the S-matrix may be viewed as trajectories in the $u-v$ plane. These S-matrix trajectories in the rhombus with physical values of the scattering lengths and with the choice $\lambda = \frac{1}{4}$ are shown in Fig. (6). The trajectories in this model are significantly more complex than the LO case and yet have clear isometries.

Here the isometries of the S-matrix trajectories are in correspondence with the UV/IR transformation on the momenta,

$$p \mapsto \frac{1}{\lambda |a_1 a_0| p} \ . \quad (2.39)$$

The action of this transformation on the coordinates and angles is

$$\begin{aligned} \underline{a_1 a_0 < 0}: \ & (x,z) \to (x,-z) \ , \ (y,w) \to (y,-w) \Longrightarrow (u,v) \to (u,-v) \ , \\ & (\phi,\theta) \to (\theta,\phi) \ , \\ \underline{a_1 a_0 > 0}: \ & (x,z) \to (x,-z) \ , \ (y,w) \to (-y,w) \Longrightarrow (u,v) \to (\bar{u},-\bar{v}) \ , \\ & (\phi,\theta) \to (-\theta,-\phi) \ . \end{aligned} \quad (2.40)$$

And the corresponding conformal invariance is again as in Eq. (2.30).

A straightforward application of the chain rule leads to the beta functions of the coordinates

$$p\frac{d}{dp}u(p) = \tfrac{1}{2}\left[\left(\tfrac{a_1(p)}{a_1} + \tfrac{a_0(p)}{a_0} - 1\right)\left(u(p)^2 + v(p)^2 - 1\right) + 2\left(\tfrac{a_1(p)}{a_1} - \tfrac{a_0(p)}{a_0}\right)uv\right] \ ; \quad (2.41)$$

$$p\frac{d}{dp}v(p) = \tfrac{1}{2}\left[\left(\tfrac{a_1(p)}{a_1} - \tfrac{a_0(p)}{a_0}\right)\left(u(p)^2 + v(p)^2 - 1\right) + 2\left(\tfrac{a_1(p)}{a_1} + \tfrac{a_0(p)}{a_0} - 1\right)uv\right] \ . \quad (2.42)$$

[8] Note that the S-matrix is, by construction, unitary to all orders in the ERE. While it is sometimes convenient in low-energy nucleon-nucleon scattering to treat effective range corrections in perturbation theory [10, 11] —which leads to an S-matrix that satisfies perturbative unitarity— this is not done here.

[9] Note that in the singly-bound case, only one effective range will be positive in this model, in violation of the Wigner bound [29–31].

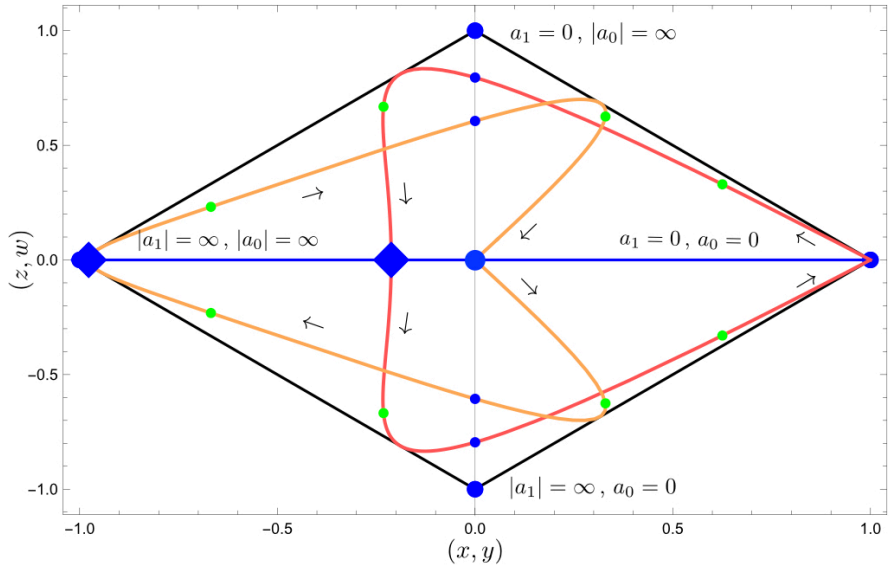

Figure 6. Rhombus in the $u - v$ plane with fixed points at the vertices and the origin. The solid red curve corresponds to the real part of $\hat{\mathbf{S}}$, and the solid orange curve corresponds to the imaginary part of $\hat{\mathbf{S}}$ at NLO in the ERE, with the physical values of the nucleon-nucleon scattering lengths and $\lambda = \frac{1}{4}$. The blue diamonds corresponds to the fixed point of the UV/IR conformal transformation. The green (blue) dots are the maxima (minima) of the EP.

And consequently S-matrix momentum flow is given by

$$p\frac{d}{dp}\hat{\mathbf{S}} = \tfrac{1}{2}\left(\hat{\mathbf{S}}^2 \;-\; \hat{\mathbf{1}}\right)\left[\left(\tfrac{a_1(p)}{a_1} + \tfrac{a_0(p)}{a_0} - 1\right)\hat{\mathbf{1}} + \left(\tfrac{a_1(p)}{a_1} - \tfrac{a_0(p)}{a_0}\right)\left(\hat{\mathbf{1}} + \hat{\boldsymbol{\sigma}}\cdot\hat{\boldsymbol{\sigma}}\right)/2\right] . \quad (2.43)$$

This momentum-flow equation reduces to LO in the ERE when $\lambda = 0$.

The EP is given by

$$\mathcal{E}(\hat{\mathbf{S}}) = 4N_{\mathcal{P}}\frac{p^2\,(a_0 - a_1)^2\left(1 + a_1a_0\lambda p^2\right)^2\left[1 + p^2\left(a_0a_1 - \left(a_1^2 + a_0^2\right)\lambda + a_1^2a_0^2\lambda^2p^2\right)\right]^2}{\left[1 + a_0^2p^2\left(1 - \lambda\left(2 - a_0^2\lambda p^2\right)\right)\right]^2\left[1 + a_1^2p^2\left(1 - \lambda\left(2 - a_1^2\lambda p^2\right)\right)\right]^2} , \quad (2.44)$$

and can be written in terms of the S-matrix beta functions as

$$\mathcal{E}(\hat{\mathbf{S}}) = 4N_{\mathcal{P}}\left|\, c_-(p)\;\beta_u(p) \;+\; c_+(p)\;\beta_v(p)\,\right|^2 , \quad (2.45)$$

where

$$c_\pm(p) \equiv \pm\frac{\left[\,(2a_0a_1(p) - a_1a_0) \pm (2a_1a_0(p) - a_1a_0)\,\right]}{2\,(2a_1(p) - a_1)\,(2a_0(p) - a_0)} . \quad (2.46)$$

The EP is plotted in Fig. (7) with the physical values of the scattering lengths and $\lambda = \frac{1}{4}$. Again the EP is conformally invariant. With physical values of the scattering lengths, there are now three zeros of the EP corresponding to the crossing of the fixed point of the conformal transformation and the crossing of the $u = 0$ line of zero entanglement.

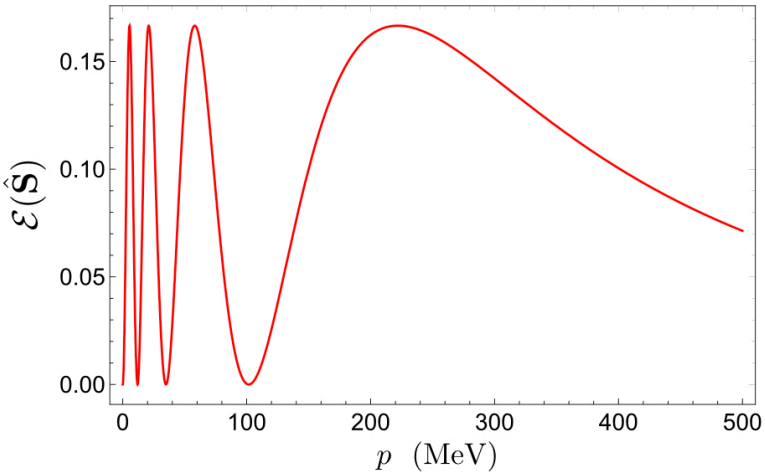

Figure 7. The EP obtained from Eq. (2.44) with the physical values of the scattering lengths and $\lambda = \frac{1}{4}$.

3 Geometry of the S-matrix

3.1 Hilbert-Schmidt Distance

The analysis of Section 2 relies on choosing a specific isotropic coordinate system to study the geometry of the S-matrix. As the S-matrix is an operator in the product Hilbert space of nucleon spins, it is interesting to consider distance measures in a basis-independent manner. For this purpose it is convenient to make use of the Hilbert-Schmidt (HS) distance. The HS distance measure is a natural extension of the Froebenius inner product, $\langle \hat{\mathbf{A}}, \hat{\mathbf{B}} \rangle = \mathrm{Tr}[\hat{\mathbf{A}}^\dagger \hat{\mathbf{B}}]$. It can be defined as [32]

$$D(\hat{\mathbf{A}}, \hat{\mathbf{B}})^2 \equiv d_n \mathrm{Tr}\left[(\hat{\mathbf{A}} - \hat{\mathbf{B}})(\hat{\mathbf{A}} - \hat{\mathbf{B}})^\dagger \right] \tag{3.1}$$

with d_n an arbitrary normalization constant that will be set to $\frac{1}{2}$. The HS distance is independent of basis, positive semi-definite and zero if and only if $\hat{\mathbf{A}} = \hat{\mathbf{B}}$. If the S-matrix is parameterized by phase shifts, say ϕ and θ, then the HS distance induces a metric on the space of S-matrices. This allows for the direct study of the geometry of the S-matrix. The HS distance between two S-matrices with distinct phase shifts, $\hat{\mathbf{S}}(\phi, \theta)$ and $\hat{\mathbf{S}}'(\phi', \theta')$, is

$$D(\hat{\mathbf{S}}, \hat{\mathbf{S}}')^2 = \tfrac{1}{2}\mathrm{Tr}\left[(\hat{\mathbf{S}} - \hat{\mathbf{S}}')(\hat{\mathbf{S}} - \hat{\mathbf{S}}')^\dagger \right] = 2\Big(\sin^2\left(\tfrac{1}{2}(\phi - \phi')\right) + 3\sin^2\left(\tfrac{1}{2}(\theta - \theta')\right) \Big) \ . \tag{3.2}$$

The metric is obtained by looking at the infinitesimal differences, $d\phi = \phi' - \phi$ and $d\theta = \theta' - \theta$ and is found to be,

$$ds^2 = \tfrac{1}{2}\left(3\, d\theta^2 + d\phi^2\right) \ . \tag{3.3}$$

The unitary S-matrix is determined by the two degrees of freedom, ϕ and θ, and therefore, locally, the S-matrix lives on the space defined by this two-dimensional Euclidean metric

that can be rescaled to remove the anisotropic spin weighting factor of the spin-triplet phase shift θ. A more geometrical approach to obtaining this metric, using an embedding, will be pursued in the next section.

The HS distance allows a definition of the analog of the "Hamiltonian operator" which governs momentum flow of the S-matrix. As a result of unitarity, two S-matrices, $\hat{\mathbf{S}}(p)$ and $\hat{\mathbf{S}}'(p+dp)$, that are infinitesimally close to each other in the two-dimensional Euclidean space are related by,

$$\hat{\mathbf{S}}' = \hat{\mathbf{S}}(\hat{\mathbf{1}} + i\,dp\,\hat{\mathbf{H}}) \ , \tag{3.4}$$

where $\hat{\mathbf{H}}$ is a Hermitian matrix. The differential line element between $\hat{\mathbf{S}}$ and $\hat{\mathbf{S}}'$ can be expressed in terms of the Froebenius norm as,

$$ds^2 = \tfrac{1}{2} dp^2 \langle \hat{\mathbf{H}}, \hat{\mathbf{H}} \rangle \ . \tag{3.5}$$

Therefore, the arc-length along a curve is

$$\frac{1}{2} \int dp \sqrt{\langle \hat{\mathbf{H}}(p), \hat{\mathbf{H}}(p) \rangle} \ . \tag{3.6}$$

Geodesics are curves between two points on the space that minimize this arc-length.

From Eq. (3.4) it follows that any S-matrix trajectory can be built up from continuous multiplication of the identity matrix at $p = 0$ by $\hat{\mathbf{1}} + i\,dp\,\hat{\mathbf{H}}(p)$. In the limit that $dp \to 0$ the S-matrix trajectory is given by,

$$\hat{\mathbf{S}}(p) = \lim_{dp \to 0} \hat{\mathbf{S}}(0) \prod_{n=1}^{n=\frac{p}{dp}} \Big(\hat{\mathbf{1}} + i\,dp\,\hat{\mathbf{H}}((n-1)\,dp) \Big) \ = \ \hat{\mathbf{1}}\,\mathcal{P}\{ e^{i \int_0^p dp' \hat{\mathbf{H}}(p')} \} \ , \tag{3.7}$$

where $\mathcal{P}$ acts as the momentum-ordering operator. Here the unitary S-matrix is analogous to the unitary time-evolution operator. The initial S-matrix is the fixed point $\hat{\mathbf{S}}(p = 0)$ and the momentum evolution propagates the system to another fixed point via the $\hat{\mathbf{H}}$ operator. It is straightforward to obtain

$$\hat{\mathbf{H}}(p) = \frac{1}{2} \Big(\dot{\phi} + \dot{\theta} \Big) \hat{\mathbf{1}} \ + \ \frac{1}{2} \Big(\dot{\phi} - \dot{\theta} \Big) \left(\hat{\mathbf{1}} + \hat{\boldsymbol{\sigma}} \cdot \hat{\boldsymbol{\sigma}} \right) / 2 \tag{3.8}$$

where the dot denotes differentiation with respect to p.

3.2 Entanglement power as a distance measure

The HS distance also serves to obtain an operator definition and an alternate understanding of the EP. Recall that the S-matrix is non-entangling when either $\phi = \theta$ or $\phi = \theta \pm \pi$ [10].

[10] When $\phi = \theta \pm \pi$ the S-matrix acts as a swap gate on the incoming nucleon-nucleon state up to an overall phase. Likewise, when $\phi = \theta \pm \frac{\pi}{2}$, the S-matrix acts as a root-swap gate on the incoming nucleon-nucleon state up to an overall phase.

Therefore, the non-entangling S-matrices form a codimension-one subspace within the space of all possible S-matrices. The EP of a given S-matrix, $\hat{\mathbf{S}}(\phi,\theta)$, is found to be,

$$\mathcal{E}(\hat{\mathbf{S}}) = D(\hat{\mathbf{S}}(\phi,\theta),\hat{\mathbf{S}}(\theta,\theta))^2\, D(\hat{\mathbf{S}}(\phi,\theta),\hat{\mathbf{S}}(\theta-\pi,\theta))^2 = N_p \sin^2(\phi-\theta)\ , \tag{3.9}$$

where the freedom in defining the HS norm has been used to set the normalization to N_p. As both $\hat{\mathbf{S}}(\theta,\theta)$ and $\hat{\mathbf{S}}(\theta-\pi,\theta)$ are non-entangling, the EP can be interpreted as a measure of the distance from a given S-matrix to the two non-entangling subspaces. Using the HS distance highlights the fact that the EP of an operator is a state-independent measure of entanglement.

3.3 Embedding in $\mathbb{R}^4$

While the HS distance provides a metric on the space of S-matrices, it is convenient to view the two-dimensional space on which the S-matrix propagates as a geometric embedding in a higher-dimensional space. Recall that in the chosen isotropic coordinates, the first unitarity constraint determines a three-sphere of fixed radius ($r = 1$):

$$x^2 \ + \ y^2 \ + \ z^2 \ + \ w^2 \ = \ r^2\ . \tag{3.10}$$

The isometry group of the three-sphere, S^3, is $SO(4)$ which is also the isometry group of $\mathbb{R}^4$. The six $SO(4)$ generators can be constructed by considering the rotations in the six planes that can be formed from the four Cartesian coordinates. The second unitarity constraint, Eq. (2.11), can be expressed in the two equivalent forms

$$(x \pm z)^2 \ + \ (y \pm w)^2 \ = \ r^2\ . \tag{3.11}$$

This leaves invariant two independent $SO(2)$ transformations. In addition, there are six discrete $\mathbb{Z}_2$ symmetries. Therefore, the isometry group of the two-dimensional space on which the S-matrix propagates is

$$SO(2) \otimes SO(2) \otimes \mathbb{Z}_2^6\ . \tag{3.12}$$

These symmetries will be given explicitly in the next subsection.

As an embedding in $\mathbb{R}^4$, with metric

$$ds^2 \ = \ dx^2 \ + \ dy^2 \ + \ dz^2 \ + \ dw^2\ , \tag{3.13}$$

and with coordinate choice give in Eq. (2.16), one finds the flat two-dimensional Euclidean metric

$$ds^2 \ = \ \tfrac{1}{2}\ \left(d\phi^2 \ + \ d\theta^2\right)\ , \tag{3.14}$$

with $\phi \in [0, 2\pi]$ and $\theta \in [0, 2\pi]$. This metric describes the flat torus $\mathbb{T}^2 \sim S^1 \otimes S^1 \in \mathbb{R}^4$, where S^1 is the circle with isometry group $SO(2)$.[11]

[11] The flat torus also shows up in the construction of the Hilbert space of two qubits. See, for example, Ref. [33].

3.4 Flat torus isometry group

Here the action of the isometry group on the variables ϕ and θ will be given explicitly. As $SO(4) \sim SU(2) \otimes SU(2)$, the generators of $SO(4)$ may be given by the generators of the two $SU(2)$'s, say X_i and Y_j with $i, j = 1, 2, 3$. The two $SO(2)$ isometries of the flat torus are then generated by X_3 ($\equiv SO(2)_-$) and Y_1 ($\equiv SO(2)_+$), where X_3 is a simultaneous rotation in the $x - y$ and $z - w$ plane by the same amount, while Y_1 is a simultaneous rotation in the $x - w$ and $y - z$ plane by opposite amounts. The action of X_3 and Y_1 on the angles ϕ and θ are given in Table 1. Note that these are these are simply the translational symmetries that one

$SO(2)_-$	X_3	$\phi \mapsto \phi + \epsilon$	$\theta \mapsto \theta + \epsilon$
$SO(2)_+$	Y_1	$\phi \mapsto \phi + \epsilon$	$\theta \mapsto \theta - \epsilon$

Table 1. Continuous isometries of the flat torus.

would expect on a flat manifold. The action of the six $\mathbb{Z}_2$ symmetries on the angles ϕ and θ are given in Table 2. It is clear that the UV/IR conformal symmetries of the LO in the ERE

a	- + - +	$\phi \mapsto \pi - \phi$	$\theta \mapsto \pi - \theta$
b	+ - + -	$\phi \mapsto -\phi$	$\theta \mapsto -\theta$
c	+ + - -	$\phi \mapsto \theta$	$\theta \mapsto \phi$
d	+ - - +	$\phi \mapsto -\theta$	$\theta \mapsto -\phi$
e	- + + -	$\phi \mapsto \pi - \theta$	$\theta \mapsto \pi - \phi$
f	- - + +	$\phi \mapsto \pi + \theta$	$\theta \mapsto \pi + \phi$

Table 2. Discrete isometries of the flat torus. Here $(+ - +-)$ corresponds to $(x, y, z, w) \mapsto (x, -y, z, -w)$, *etc.* Note that the signs of all values of π are arbitrary.

and in the conformal range model are in correspondence with discrete flat-torus isometries. This will be important in what follows.

4 S-matrix theory of scattering

4.1 Action principle

The s-wave nucleon-nucleon S-matrix is a one-dimensional trajectory that lives on a flat torus, which is a two-dimensional Euclidean space with periodic boundary conditions on the two phase-shift coordinates. Straight line trajectories on this flat space are geodesics, which are formally obtained by minimizing an action which represents a path in the space. In general, S-matrix trajectories will not be geodesics and therefore external forces must be present. The action for a general parameterization[12] of a curve on a space with metric tensor g_{ab} can be taken as [34]

$$\int L\left(\mathcal{X}, \dot{\mathcal{X}}\right) d\sigma \;=\; \int \left(\mathbf{N}^{-2} g_{ab} \dot{\mathcal{X}}^a \dot{\mathcal{X}}^b \;-\; \mathbb{V}(\mathcal{X})\right) \mathbf{N} d\sigma \tag{4.1}$$

[12]Note that this form avoids the square root in the Lagrangian while allowing inaffine parameterizations.

where σ is the parameter (affine or inaffine), $\dot{\mathcal{X}} \equiv d\mathcal{X}/d\sigma$, and $\mathbb{V}(\mathcal{X})$ is an external potential which is assumed to be a function of $\mathcal{X}$ only[13]. Minimizing the action or equivalently solving the Euler-Lagrange equations gives the trajectory equation

$$\ddot{\mathcal{X}}^a \;+\; {}_g\Gamma^a{}_{bc}\dot{\mathcal{X}}^b\dot{\mathcal{X}}^c \;=\; \kappa(\sigma)\dot{\mathcal{X}}^a \;-\; \tfrac{1}{2}\mathbf{N}^2 g^{ab}\partial_b\mathbb{V}(\mathcal{X}) \;, \tag{4.2}$$

where ${}_g\Gamma^a{}_{bc}$ are the Christoffel symbols for the metric g_{ab}, and

$$\kappa(\sigma) \;\equiv\; \frac{\dot{\mathbf{N}}}{\mathbf{N}} = \frac{d}{d\sigma}\ln\frac{d\lambda}{d\sigma} \;. \tag{4.3}$$

Here κ is the inaffinity [35], which vanishes when $\sigma = \lambda$ with λ an affine parameter. For constant potential, the trajectory equation reduces to the geodesic equation.

4.2 Geodesics on the flat torus

With $\mathcal{X}^1 = \phi$ and $\mathcal{X}^2 = \theta$ and omitting the external force term, the equations for geodesics are then read off to be:

$$\begin{aligned} \ddot{\phi} \;&=\; \kappa(\sigma)\dot{\phi} \;\;, \\ \ddot{\theta} \;&=\; \kappa(\sigma)\dot{\theta} \;. \end{aligned} \tag{4.4}$$

In the affine case, $\sigma = \lambda$ and $\kappa = 0$, ϕ and θ are linear functions of λ, and the most general solution is a straight line in the Euclidean (ϕ-θ) plane. In the non-affine case ϕ and θ can be arbitrary functions of σ, and the most general solution is again a straight line in the Euclidean (ϕ-θ) plane. For instance, say $\phi = f(\sigma)$ and $\theta = g(\sigma)$ with f and g arbitrary differentiable functions. Then,

$$\frac{\ddot{\phi}}{\dot{\phi}} \;=\; \frac{\ddot{\theta}}{\dot{\theta}} \;=\; \kappa(\sigma) \tag{4.5}$$

implies $f = c_1 + c_2\, g$, giving the desired result. In this way, using the inaffinity, the effective range expansion can be built up to any order. For instance, to leading order, assuming that $\phi = \theta$ and $\sigma = p$, one can choose $\phi = \theta = -2\tan^{-1}(ap)$ with

$$\kappa(p) \;=\; -\frac{2a^2 p}{1 + a^2 p^2} \;. \tag{4.6}$$

At NLO in the ERE one can choose $\phi = \theta = 2\cot^{-1}\left(-\frac{1}{ap} + \frac{1}{2}rp\right)$ where r is the effective range, with a corresponding κ, and so the momentum dependence of the full phase shift may be built up by appropriate choice of inaffinity.

4.3 Entanglement forces and the ERE

Recall that the EP is

$$\mathcal{E}(\hat{\mathbf{S}}) = N_{\mathcal{P}}\, \sin^2(\phi - \theta) \;. \tag{4.7}$$

[13] This assumption will have to be relaxed when considering projections onto parts of a space.

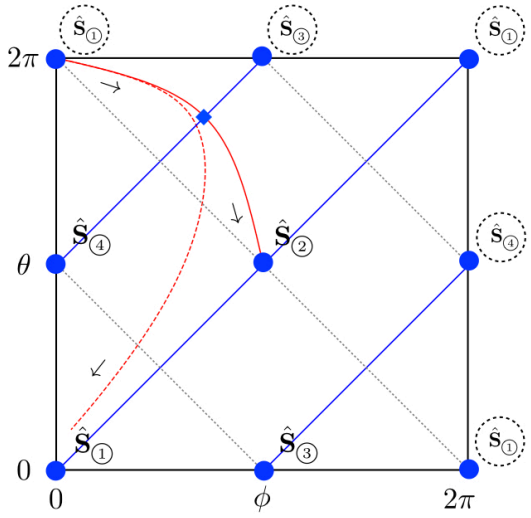

Figure 8. The S-matrix embedding in $\mathbb{R}^4$ as the flat torus. The blue dots are the RG fixed points of the S-matrix and the image fixed points are within dotted circles. All diagonal lines are geodesics. The solid blue lines are geodesics with vanishing entanglement, and the dotted black lines are geodesics with non-vanishing entanglement. The blue diamond is the fixed point of the UV/IR conformal symmetry. The physical S-matrix taken from the Nijmegen phase shift analysis [22] (PWA93) is the dashed red curve, and LO in the ERE is the solid red curve.

The EP preserves all of the discrete isometries of the flat torus, however the $SO(2)_+$ translational symmetry is broken; only translations in one direction on the flat torus preserve spin-entangling effects. The blue lines in Fig. (8) are lines of vanishing entanglement and all lines parallel are lines of equi-entanglement which are protected by the $SO(2)_-$ invariance.

Therefore in order to find a non-geodesic solution with $\phi \neq \theta + n\pi$, an external entangling force must be present. The general equation, Eq. (4.2) gives

$$\begin{aligned} \ddot{\phi} &= \kappa(\sigma)\dot{\phi} - \mathbf{N}^2\,\partial_\phi \mathbb{V}(\phi,\theta) \ , \\ \ddot{\theta} &= \kappa(\sigma)\dot{\theta} - \mathbf{N}^2\,\partial_\theta \mathbb{V}(\phi,\theta) \ . \end{aligned} \tag{4.8}$$

If a solution for ϕ and θ is specified, these two coupled equations have three unknowns given by the inaffinity and the components of the force in the two directions in the plane.

LO in the ERE

Consider LO in the ERE. With $\sigma = p$, the solution is once again

$$\phi = -2\tan^{-1}(a_0 p) \quad , \quad \theta = -2\tan^{-1}(a_1 p) \ , \tag{4.9}$$

and is exhibited in Fig. (8). (The physical trajectory with the Nijmegen phase shift analysis [22] (PWA93) is also shown.) The conformal transformation $p \mapsto (|a_1 a_0| p)^{-1}$ is in correspondence with the isometry $\mathbb{Z}_2^e$ for $a_1 a_0 > 0$ (doubly-(un)bound) and $\mathbb{Z}_2^f$ for $a_1 a_0 < 0$

(singly-bound). These isometries leave the angle $\phi + \epsilon\,\theta$ invariant with $\epsilon = -1$ for $a_1 a_0 > 0$ and $\epsilon = +1$ for $a_1 a_0 < 0$. For these isometries, $\mathbb{V}(\phi + \epsilon\theta, \phi - \epsilon\theta) = \mathbb{V}(\phi + \epsilon\theta, -(\phi - \epsilon\theta))$ and the simplest solution is $\mathbb{V}(\phi, \theta) = \mathbb{V}(\phi + \epsilon\,\theta)$. This implies $\partial_\phi \mathbb{V} = \epsilon\,\partial_\theta \mathbb{V}$, which renders the system integrable: the equations decouple to

$$\begin{aligned} \ddot{\phi} + \epsilon\,\ddot{\theta} &= \kappa\left(\dot{\phi} + \epsilon\,\dot{\theta}\right) + 2\,\mathbb{F} \ , \\ \ddot{\phi} - \epsilon\,\ddot{\theta} &= \kappa\left(\dot{\phi} - \epsilon\,\dot{\theta}\right) \ , \end{aligned} \tag{4.10}$$

where the external force is given by $\mathbb{F} \equiv -\mathbf{N}^2\,\partial_\phi \mathbb{V}$.

The inaffinity and the force are determined algebraically to be

$$\begin{aligned} \mathbf{N} &= c_1\left(\dot{\phi} - \epsilon\,\dot{\theta}\right) \quad , \quad \kappa = \left(\frac{\ddot{\phi} - \epsilon\,\ddot{\theta}}{\dot{\phi} - \epsilon\,\dot{\theta}}\right) \quad , \\ \mathbb{F} &= -\epsilon\left(\frac{\ddot{\phi}\,\dot{\theta} - \ddot{\theta}\,\dot{\phi}}{\dot{\phi} - \epsilon\,\dot{\theta}}\right) \ , \end{aligned} \tag{4.11}$$

where $c_1 > 0$ is an integration constant. In terms of the scattering lengths, one finds

$$\mathbf{N} = -\frac{2c_1\,(a_0 - \epsilon\,a_1)\left(1 - \epsilon\,a_0 a_1 p^2\right)}{\left(1 + a_0^2 p^2\right)\left(1 + a_1^2 p^2\right)} \quad , \quad \kappa(p) = -\frac{2a_0^2 p}{1 + a_0^2 p^2} - \frac{2a_1^2 p}{1 + a_1^2 p^2} - \frac{2a_0 a_1 p}{\epsilon - a_0 a_1 p^2} \ , \tag{4.12}$$

and the force is

$$\mathbb{F} = -\frac{4\epsilon\,a_0 a_1 p\left(a_1^2 - a_0^2\right)}{\left(1 + a_0^2 p^2\right)\left(1 + a_1^2 p^2\right)\left[a_1\left(1 + a_0^2 p^2\right)\epsilon - a_0\left(1 + a_1^2 p^2\right)\right]} \ . \tag{4.13}$$

The inaffinity and the entangling force are complicated non-local functions of the momentum; this is expected as locality plays no role in constraining the geometric description.

Integrating the force gives the external potential,

$$\mathbb{V}(\phi, \theta) = c_2\,\tan^2\left(\tfrac{1}{2}(\phi + \epsilon\,\theta)\right) \ , \tag{4.14}$$

where

$$c_2 = \frac{|a_0 a_1|}{\left(|a_0| + |a_1|\right)^2 c_1^2} \ . \tag{4.15}$$

With $c_1 = 1$, c_2 is a dimensionless coupling constant that ranges from 0 to 0.25. In the physical case $c_2 = 0.152$. The potential is constrained by the assumed discrete symmetries and, defined over the entire manifold, is invariant with respect to the $SO(2)_\epsilon$ translational symmetry. Therefore, only in the doubly-(un)bound case ($\epsilon = -1$), does the potential share the symmetry of the entanglement power. This asymmetry is a fundamental feature of the geometric description. The relative sign of the scattering lengths picks one preferred direction on the flat torus. However, the entanglement power universally breaks the $SO(2)_+$ isometry

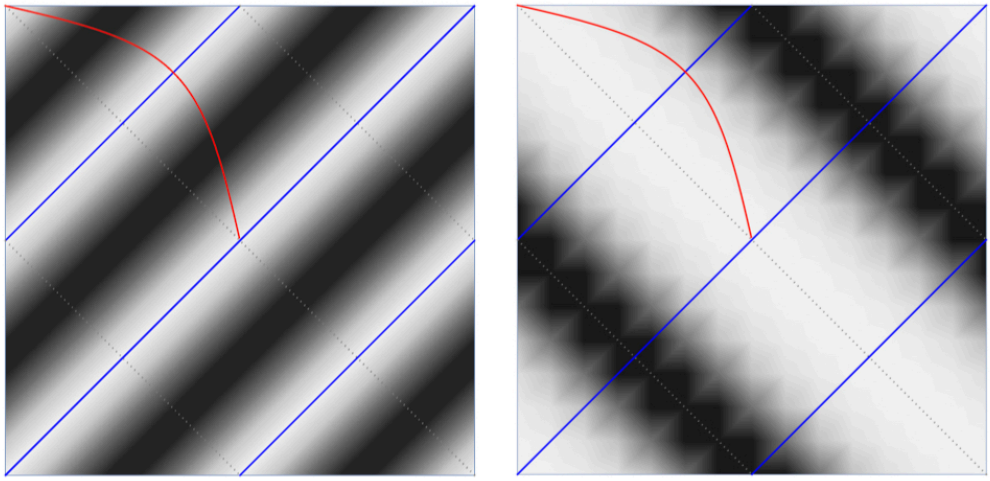

Figure 9. Heat maps on the flat torus illustrating regions of equi-entanglement and equi-potential. The red curve in both panels is the S-matrix trajectory at LO in the ERE. The EP of the S-matrix is shown in the left panel. Lighter shade indicates smaller EP. The external potential given by Eq. (4.14) is shown in the right panel. Lighter shade indicates smaller potential.

of the flat torus. Heat maps for the entanglement power and the external potential, $\mathbb{V}(\phi, \theta)$, are shown for the physical case in Fig. (9). It is worth re-considering the plot of the EP given in Fig. (3) using the heat map as a guide; the S-matrix trajectory leaves the initial fixed point, ascends to a maximum of the EP, then descends to the zero of the EP at the UV/IR conformal fixed point which lies on the blue geodesic, and then rises again to the maximum before hitting the final fixed point.

It is straightforward to understand why the potential takes the simple harmonic form of Eq. (4.14). It follows from the solution Eq. (4.9), that for any finite values of the scattering lengths, only the $\hat{\mathbf{S}}_{①}$ and $\hat{\mathbf{S}}_{②}$ fixed points (and their images) can be accessed by an S-matrix trajectory. Therefore the potential at these fixed points should be finite. And because of the symmetry implied by the condition that $\phi + \epsilon\,\theta$ be invariant, the potential must take the same constant value at each fixed point. As the $\hat{\mathbf{S}}_{③}$ and $\hat{\mathbf{S}}_{④}$ fixed points (and their images) cannot be accessed by an S-matrix trajectory, the potential should be infinite at these fixed points. (See Fig. (10).) On the flat torus, the potential must be a harmonic function and therefore these constraints imply that $\mathbb{V}$ is proportional to $\sec(\frac{1}{2}(\phi+\epsilon\,\theta))$ to some even power. Shifting the potential by a constant to give vanishing potential at the accessible fixed points then gives Eq. (4.14). If one of the channels approaches unitarity, then the potential changes form; for instance, if a_0 is taken to negative infinity and a_1 is held fixed at its physical value, then the potential vanishes and the S-matrix trajectory begins at fixed point $\hat{\mathbf{S}}_{③}$ and moves to $\hat{\mathbf{S}}_{②}$ along a geodesic.

It is convenient to define the conformal derivative and coordinates

$$D \equiv p\frac{d}{dp} \quad , \quad \overline{\mathbb{F}} \equiv p^2\,\mathbb{F} \quad , \quad \overline{\mathbb{F}}^v_a \equiv (1 \;+\; p\,\kappa)\,D\mathcal{X}_a \;. \tag{4.16}$$

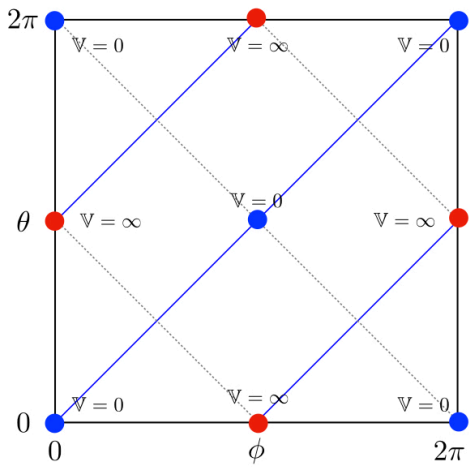

Figure 10. Discrete values of the singly-bound entangling potential on the flat torus for finite values of the scattering lengths. The potential vanishes at the blue dot fixed points and is infinite at the red dot fixed points.

The trajectory equations are then

$$\begin{aligned} D^2\phi &= \overline{\mathbb{F}}^v_\phi + \overline{\mathbb{F}} \,, \\ D^2\theta &= \overline{\mathbb{F}}^v_\phi + \epsilon\, \overline{\mathbb{F}} \,, \end{aligned} \tag{4.17}$$

which have the manifest conformal invariance

$$D \to -D \quad , \quad \phi \leftrightarrow \epsilon\theta \quad , \quad \overline{\mathbb{F}} \to \overline{\mathbb{F}} \quad , \quad \overline{\mathbb{F}}^v_\phi \leftrightarrow \epsilon \overline{\mathbb{F}}^v_\theta \,. \tag{4.18}$$

The dimensionless entangling forces in the physical case are plotted in Fig. (11). While the entangling force $\overline{\mathbb{F}}/\mathbf{N}^2$ is physical, the viscous inaffinity forces $\overline{\mathbb{F}}^v_\phi$ and $\overline{\mathbb{F}}^v_\theta$ can be altered or removed by reparameterization. However, it is critical to note that these viscous forces build the momentum variable which is the experimental knob which allows the measurement of the S-matrix.

It is straightforward to find the solution corresponding to vanishing inaffinity, described by an affine parameter λ that is unrelated to any experimental knob. In this case, the trajectory is governed by the simple Lagrangian,

$$L = \tfrac{1}{2}\left(\dot\phi + \dot\theta\right) - c_2 \tan^2\left(\tfrac{1}{2}(\phi + \epsilon\,\theta)\right) \,, \tag{4.19}$$

where the dot denotes differentiation with respect to λ. Variation of the Lagrangian gives rise to the geodesic equations

$$\begin{aligned} \ddot\phi + \epsilon\,\ddot\theta &= -\,2\,c_2\, \sec^2\left(\tfrac{1}{2}(\phi + \epsilon\,\theta)\right) \tan\left(\tfrac{1}{2}(\phi + \epsilon\,\theta)\right) \,, \\ \ddot\phi - \epsilon\,\ddot\theta &= 0 \,. \end{aligned} \tag{4.20}$$

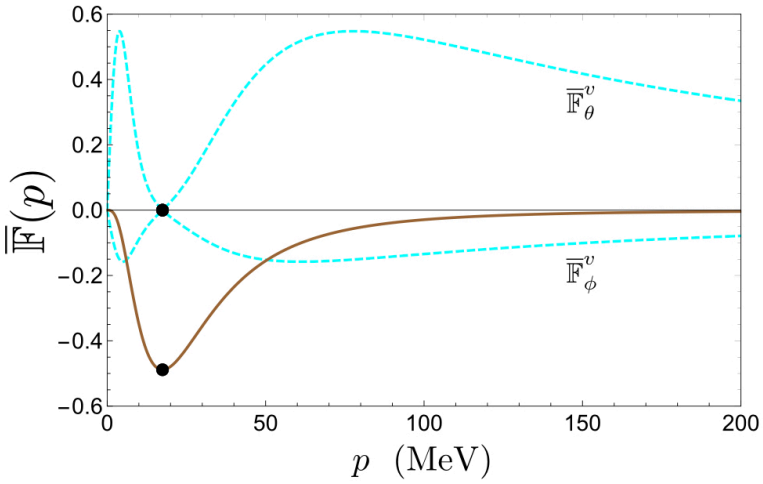

Figure 11. The dimensionless entangling force plotted versus momentum in the physical case (solid brown line). The black dot corresponds to the fixed point of the conformal transformation where the S-matrix crosses the geodesic and the EP vanishes. Also plotted are the viscous inaffinity forces (dashed cyan lines).

The affine parameter can be chosen to give the solution

$$\begin{aligned} \phi + \epsilon\,\theta &= 2\,\sin^{-1}\left(\sqrt{1-4c_2}\,\sin\frac{\lambda}{2}\right)\,, \\ \phi - \epsilon\,\theta &= \lambda\,. \end{aligned} \tag{4.21}$$

The S-matrix trajectory from fixed point $\hat{\mathbf{S}}_{①}$ to fixed point $\hat{\mathbf{S}}_{②}$ is then found to be

$$\begin{aligned} \phi(\lambda) &= \frac{1}{2}\left(2\,\mathrm{sgn}(|a_0|-|a_1|)\,\sin^{-1}\left(\left|\frac{a_0+\epsilon a_1}{a_0-\epsilon a_1}\right|\sin\frac{\lambda}{2}\right)+\lambda\right)\,, \\ \theta(\lambda) &= \frac{\epsilon}{2}\left(2\,\mathrm{sgn}(|a_0|-|a_1|)\,\sin^{-1}\left(\left|\frac{a_0+\epsilon a_1}{a_0-\epsilon a_1}\right|\sin\frac{\lambda}{2}\right)-\lambda\right)\,, \end{aligned} \tag{4.22}$$

where c_2 has been fixed to match the inaffine solution at the conformal fixed point (and is consistent with Eq. (4.15) with $c_1 = 1$). This S-matrix trajectory is exactly equivalent to LO in the ERE.

Conformal range model

Consider now the solution of the conformal range model

$$\phi = -2\tan^{-1}\left(\frac{a_0 p}{1-\lambda a_0^2 p^2}\right) \quad,\quad \theta = -2\tan^{-1}\left(\frac{a_1 p}{1-\lambda a_1^2 p^2}\right)\,, \tag{4.23}$$

which is exhibited on the flat torus in Fig. (12) in the case of physical scattering lengths and $\lambda = 1/4$. The conformal transformation $p \mapsto (\lambda|a_1 a_0|p)^{-1}$ is in correspondence with the isometry $\mathbb{Z}_2^d$ for $a_1 a_0 > 0$ and $\mathbb{Z}_2^c$ for $a_1 a_0 < 0$. These isometries again leave the angle $\phi + \epsilon\,\theta$

invariant with $\epsilon = -1$ for $a_1 a_0 > 0$ and $\epsilon = +1$ for $a_1 a_0 < 0$. Therefore the algebraic form of the solution is identical to what we found in the LO ERE, i.e. Eq. (4.11). For arbitrary values of λ the entangling potential is cumbersome. However, in the special case $\lambda = 1/4$ the potential reduces to

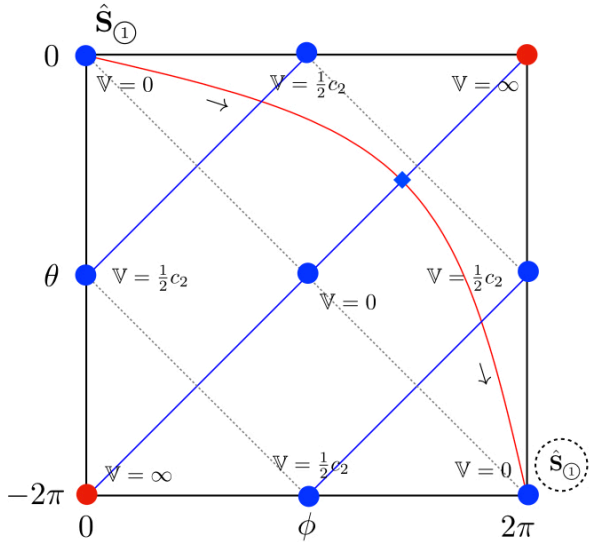

Figure 12. The S-matrix trajectory in the conformal range model on the flat torus. Physical values of the scattering lengths and $\lambda = 1/4$ have been used. The blue diamond is the fixed point of the UV/IR conformal symmetry. The blue dots are the fixed points of the S-matrix and the image fixed points are within dotted circles. All diagonal lines are geodesics. The solid blue lines are geodesics with vanishing entanglement, and the dotted black lines are geodesics with non-vanishing entanglement.

$$\mathbb{V}(\phi, \theta) = \tfrac{1}{2}c_2 \, \tan^2\left(\tfrac{1}{4}(\phi + \epsilon\,\theta)\right) \ . \tag{4.24}$$

It is clear from the solution of Eq. (4.23) that only the $\hat{\mathbf{S}}_{①}$ trivial fixed point and its image can be reached by an S-matrix trajectory. Fig. (12) indicates discrete values of the potential on the flat torus. Note that this potential is periodic only by a shift of $\phi + \epsilon\,\theta$ by 4π, in contrast with the LO ERE potential.

5 Inelasticity and holography

5.1 Inelasticity and the bulk

So far it has been assumed that all inelastic thresholds in the scattering process have been pushed to infinity so that the S-matrix is unitary and defined for all (positive) center-of-mass momenta p. One might imagine controlling the inelasticity in nucleon-nucleon scattering by varying the light-quark masses in QCD to adjust the threshold for pion production. In the chiral limit, at scattering threshold there will be pion radiation which, for present purposes, is not measured and is removed from the system as a loss of unitarity. In the S-matrix

formalism, the inclusion of some generic inelastic scattering process is achieved by replacing the single-channel S-matrices by $\eta_0 \exp 2i\delta_0$ and $\eta_1 \exp 2i\delta_1$, with the inelasticity parameters satisfying $0 < \eta_{0,1} < 1$. Assuming here that $\eta_0 = \eta_1 = r$, inelasticity can be realized in the $\mathbb{R}^4$ embedding coordinates of Eq. (2.16) through variation of r[14]. The S-matrix with inelasticities present, $\hat{\mathbf{S}}_I$, then satisfies the formal relation

$$\hat{\mathbf{S}}_I^\dagger \hat{\mathbf{S}}_I \;=\; \hat{\mathbf{S}}^\dagger \hat{\mathbf{S}} \;-\; \sum_\gamma |\gamma\rangle\langle\gamma| \;, \tag{5.1}$$

where $\hat{\mathbf{S}}$ is the unitary S-matrix of the total system (nucleon-nucleon and inelastic channels), and γ represents an inelastic contribution. It then follows that

$$\left(1 \;-\; r^2\right)\; \hat{\mathbf{1}} = \sum_\gamma |\gamma\rangle\langle\gamma| \;. \tag{5.2}$$

It is clear that, in general, r depends in a complicated way on momentum and involves a summation over all kinematically-allowed final states. In the nucleon-nucleon system, the leading inelasticities arise from pion production, which in principle is calculable using chiral-perturbation theory methods. So for instance, the excluded states may be of the form

$$\sum_\gamma |\gamma\rangle\langle\gamma| = |NN\pi\rangle\langle NN\pi| \;+\; \ldots \;+\; |NN\pi\ldots\pi\rangle\langle NN\pi\ldots\pi| \;+\; \ldots \;. \tag{5.3}$$

The momentum flow equation with inelasticities present is

$$p\frac{d}{dp}\hat{\mathbf{S}}_I \;=\; r\;\left(p\frac{d}{dp}\hat{\mathbf{S}} \;+\; \left(p\frac{d}{dp}\ln r\right)\hat{\mathbf{S}}\right) \;. \tag{5.4}$$

In addition to the four RG fixed points on the unitary boundary at $r = 1$, there is now an additional fixed point at $r = 0$. All the fixed points have vanishing spin entanglement as the EP generalizes to

$$\mathcal{E}(\hat{\mathbf{S}}_I) \;=\; N_{\mathcal{P}}\; r^4 \sin^2\left(\phi - \theta\right) \;, \tag{5.5}$$

which drops off rapidly when $r < 1$.

5.2 Embedding in $\mathbb{R}^4$

With the three coordinates $\mathcal{X}^1 = r$, $\mathcal{X}^2 = \phi$, and $\mathcal{X}^3 = \theta$ embedded in $\mathbb{R}^4$, the metric of the bulk space takes the form

$$ds^2 \;=\; dr^2 \;+\; \tfrac{1}{2}\, r^2\left(d\phi^2 \;+\; d\theta^2\right) \;, \tag{5.6}$$

with flat-torus boundary at $r = 1$. The hyperbolic space described by this metric has scalar curvature

$$R \;=\; -\frac{2}{r^2} \;. \tag{5.7}$$

[14]Note that the assumption that the two channels couple to the same source of inelasticity is critical; if η_0 and η_1 are allowed to vary independently then the resulting geometry is radically different.

There is therefore a singularity[15] at the fixed point $r = 0$ where there is total loss of unitarity and vanishing EP. The Einstein tensor has one non-vanishing component given by

$$G_{11} \;=\; \frac{1}{r^2}\;. \tag{5.8}$$

Therefore the bulk metric solves the Einstein equation[16]

$$G_{ij} \;=\; \frac{1}{r^2}\delta^1_i\delta^1_j\;. \tag{5.9}$$

It is worth emphasizing again that this singular hyperbolic geometry results as a consequence of the assumption that the inelasticity in the two channels of scattering are correlated. If η_0 and η_1 are taken to be independent, then the resulting embedding simply yields a parametric representation of the flat four-dimensional Euclidean space, $\mathbb{R}^4$.

5.3 Geodesics in the bulk

An interesting question is whether the S-matrix trajectories on the boundary can be recovered in the bulk space. That is, is it possible to engineer a bulk potential which gives a bulk trajectory which in turn reproduces the boundary trajectory corresponding to LO in the ERE? (An illustration is provided in Fig. (13)). Trajectories on the flat-torus boundary are unitary, by construction, and are in correspondence with local interactions in the EFT. By contrast, inelastic effects are in correspondence with non-local interactions in the EFT. Geodesics in both affine and inaffine parameterizations will be considered first, as the construction of these solutions enables a straightforward engineering of the potential which governs the trajectories in the LO ERE solution.

In the absence of entangling forces and inaffinity, the geodesic equations in the affine parameter λ are:

$$\ddot{r} = \tfrac{1}{2}r[(\dot{\phi})^2 \;+\; (\dot{\theta})^2] \;\;,\;\; \ddot{\phi} \;=\; -\,2\dot{\phi}\,\tfrac{\dot{r}}{r} \;\;,\;\; \ddot{\theta} \;=\; -\,2\dot{\theta}\,\tfrac{\dot{r}}{r}\;. \tag{5.10}$$

The general solution to these equations is straightforward to find. Consider the special S-matrix trajectory from fixed point $\hat{\mathbf{S}}_{①}$ to fixed point $\hat{\mathbf{S}}_{②}$ with $\phi = \theta$. On the flat-torus, this trajectory moves along a non-entangling geodesic. In the bulk, the corresponding geodesic is

$$\begin{aligned} r(\lambda) \;&=\; \sqrt{1 + (4-\delta)\,\lambda\,(\lambda-1)}\;, \\ \phi(\lambda) = \theta(\lambda) \;&=\; \tan^{-1}\left(\frac{\lambda\sqrt{\delta\,(4-\delta)}}{2-\lambda\,(4-\delta)}\right)\;, \end{aligned} \tag{5.11}$$

where $\lambda \in [0,1]$ and δ is a small parameter. The boundary geodesic is recovered in the limit $\delta \to 0$ where the trajectory goes through the singularity and there is a discontinuity at the

[15] The Kretschmann scalar is given by $K = R^{ijkl}R_{ijkl} = R^2 = 4/r^4$.

[16] This solution is reminiscent of Vaidya metrics in spacetime, which are generalizations of the Schwarzschild metric with time-dependent mass function, and describe null dust forming a black hole [35].

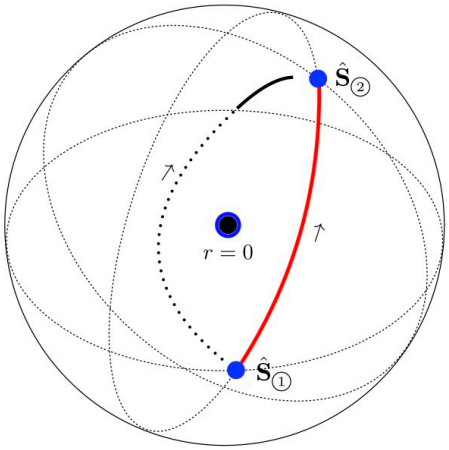

Figure 13. Bulk space with flat torus on the boundary. The unitary S-matrix lives on the flat-torus boundary and here corresponds to the (solid red) trajectory between the RG fixed points. The bulk (dotted black) trajectory begins on the boundary and through inelastic loss enters the bulk, while avoiding the singularity, and then comes back out to the boundary without quite reaching the fixed point.

half-way point $\lambda = 1/2$:

$$\begin{aligned} r(\lambda) &= 2|\lambda - \tfrac{1}{2}| \ , \\ \phi(\lambda) = \theta(\lambda) &= \pi\,\Theta\left(\lambda - \tfrac{1}{2}\right) \ , \end{aligned} \tag{5.12}$$

where $\Theta(x)$ is the Heaviside step function. Avoidance of the singularity requires non-vanishing δ and incurs an error in ϕ of order $\sqrt{\delta}$. The affine solutions are plotted for various values of δ in Fig. (14).

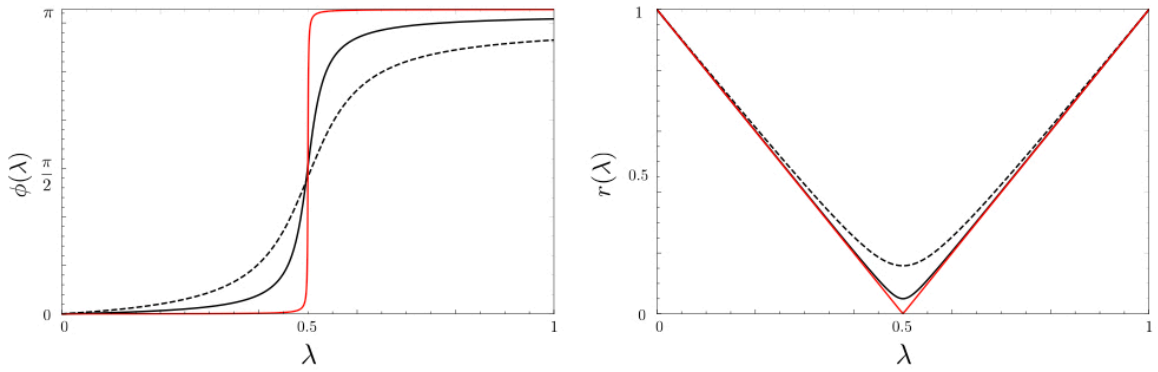

Figure 14. Affinely parameterized bulk geodesic between S-matrix fixed points. The dashed (solid) black line corresponds to $\delta = 0.1$ (0.01). The red curve is approaching the discontinuous limit $\delta \to 0$.

Consider now parameterizing the same geodesic with the non-affine parameter σ. The

geodesic equations are

$$\begin{aligned}
\ddot{r} &= \hat{\kappa}(\sigma)\dot{r} \;+\; \tfrac{1}{2}r[(\dot{\phi})^2 \;+\; (\dot{\theta})^2] \;\;, \\
\ddot{\phi} &= \hat{\kappa}(\sigma)\dot{\phi} \;-\; 2\dot{\phi}\,\frac{\dot{r}}{r} \;\;, \\
\ddot{\theta} &= \hat{\kappa}(\sigma)\dot{\theta} \;-\; 2\dot{\theta}\,\frac{\dot{r}}{r} \;\;.
\end{aligned} \tag{5.13}$$

Choosing the inaffinity to be

$$\hat{\kappa}(\sigma) = \frac{\dot{\hat{N}}}{\hat{N}} \;=\; \kappa(\sigma) \;+\; 2\frac{\dot{r}}{r} \;, \tag{5.14}$$

with κ the inaffinity of the boundary solution given in Eq. (4.6), then the ϕ and θ trajectory equations in Eq. (5.13) are satisfied with $\phi = \theta = -2\tan^{-1}(\sigma)$. However, then the first equation is solved to give

$$r(\sigma) = \frac{1+\sigma^2}{(1-\sigma^2)+e_1\sigma} \;, \tag{5.15}$$

where e_1 is an integration constant. Note that r never approaches the singularity. While $r(0) = 1$, and therefore the geodesic begins on the boundary, as $\sigma \to \infty$, $r(\sigma) \to -1$. Since $0 < r \leq 1$, the solution is sensible only up to a cutoff value of σ, $\sigma_{\text{MAX}} = \frac{e_1}{2}$. Then, ϕ and θ only reach the fixed point up to a correction given by $2/\sigma_{\text{MAX}}$. The inaffine solutions are plotted for various values of σ_{MAX} in Fig. (15). By integrating the inaffinity, it is straightforward to relate the affine and inaffine parameterizations[17]. These results provide evidence that, for non-entangling geodesics, the S-matrix can be recovered by going through the bulk, up to a quantifiable error.

5.4 Recovery of the ERE and error correction

In the presence of an external potential, $\hat{\mathbb{V}}(r,\phi,\theta)$, with the parameter choice $\sigma = p$, the trajectory equations are

$$\begin{aligned}
\ddot{r} &= \hat{\kappa}(p)\dot{r} \;+\; \tfrac{1}{2}r[(\dot{\phi})^2 \;+\; (\dot{\theta})^2] \;-\; \tfrac{1}{2}\hat{N}^2\partial_r\hat{\mathbb{V}} \;, \\
\ddot{\phi} &= \hat{\kappa}(p)\dot{\phi} \;-\; 2\dot{\phi}\,\frac{\dot{r}}{r} \;-\; \hat{N}^2\frac{1}{r^2}\partial_\phi\hat{\mathbb{V}} \;, \\
\ddot{\theta} &= \hat{\kappa}(p)\dot{\theta} \;-\; 2\dot{\theta}\,\frac{\dot{r}}{r} \;-\; \hat{N}^2\frac{1}{r^2}\partial_\theta\hat{\mathbb{V}} \;.
\end{aligned} \tag{5.17}$$

Choosing the inaffinity as in Eq. (5.14) but now with N given by the LO ERE solution, one finds $\hat{N} = r^2 N$. The LO ERE solution of Eq. (2.27) for ϕ and θ is then recovered with

[17] One finds

$$\lambda \;=\; \frac{\sigma(1+\sigma_{\text{MAX}}^2)}{\sigma_{\text{MAX}}(1-\sigma^2+2\sigma\sigma_{\text{MAX}})} \;, \tag{5.16}$$

with $\delta = 1/(1+\sigma_{\text{MAX}}^2)$.

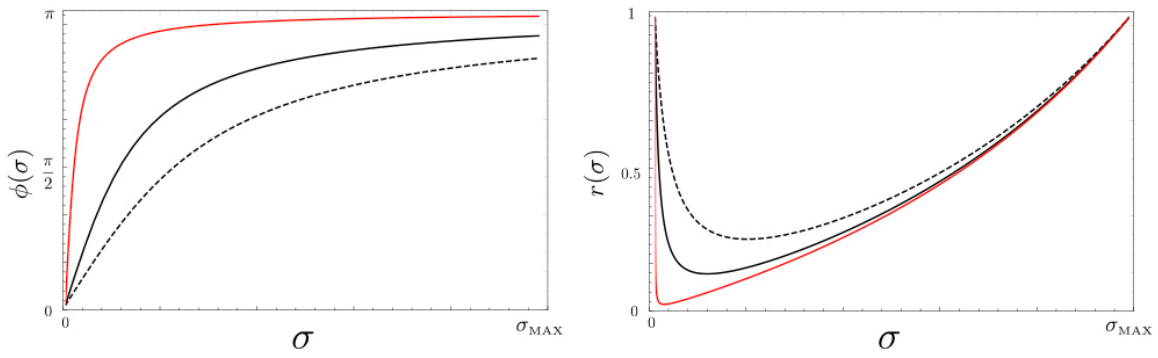

Figure 15. Inaffinely parameterized bulk geodesic between S-matrix fixed points. The dashed (solid) black line corresponds to $\sigma_{\text{MAX}} = 4$ (8). The red curve corresponds to $\sigma_{\text{MAX}} = 50$.

external potential (with the choice $c_1 = 1$)

$$\hat{\mathbb{V}}(r,\phi,\theta) = \frac{1}{r^2}\mathbb{V}(\phi,\theta) \;=\; \frac{|a_0 a_1|}{(|a_0|+|a_1|)^2}\,\frac{1}{r^2}\,\tan^2\left(\tfrac{1}{2}(\phi+\epsilon\,\theta)\right)\;. \tag{5.18}$$

The bulk entangling potential is therefore proportional to the source of the scalar curvature of the hyperbolic space. The differential equation for $r(p)$ is

$$\ddot{r} = \left(\kappa(p) + 2\frac{\dot{r}}{r}\right)\dot{r} \;+\; \tfrac{1}{2}r\left[(\dot{\phi})^2 \;+\; (\dot{\theta})^2 \;+\; 2N^2\mathbb{V}\right]\;. \tag{5.19}$$

The relevant solution is

$$r(p) \;=\; \cos\left(\mathcal{A}\tfrac{1}{2}(\phi_{\text{max}} - \epsilon\,\theta_{\text{max}})\right)\sec\left(\mathcal{A}\left[(\phi(p) - \epsilon\,\theta(p)) \;-\; \tfrac{1}{2}(\phi_{\text{max}} - \epsilon\,\theta_{\text{max}})\right]\right)\;, \tag{5.20}$$

where $\phi_{\text{max}} = \phi(p_{\text{max}})$, $\theta_{\text{max}} = \theta(p_{\text{max}})$, and

$$\mathcal{A} \;\equiv\; \frac{\sqrt{a_0^2 + a_1^2}}{\sqrt{2}(a_0 - \epsilon a_1)}\;. \tag{5.21}$$

Note that $r(0) = r(p_{\text{max}}) = 1$. Unlike the geodesic case, there is now a maximum value of p_{max} beyond which the singularity is reached. This occurs when

$$\mathcal{A}\,(\phi_{\text{max}} - \epsilon\,\theta_{\text{max}}) = -\pi\;. \tag{5.22}$$

In the physical case this gives the bound $p_{\text{max}} < 89.4$ MeV. Therefore, there is an intrinsic error in reproducing the physical S-matrix —that is $\phi(p)$ and $\theta(p)$— from bulk data as the fixed point values of $\pm\pi$ can never be reached. Indeed, one finds at p_{max}:

$$\begin{aligned}
\phi &= \pi \;+\; \frac{2}{a_0 p_{\text{max}}} \;+\mathcal{O}\left((a_0 p_{\text{max}})^{-3}\right) \;=\; 0.94\,\pi\;,\\
\theta &= -\pi \;+\; \frac{2}{a_1 p_{\text{max}}} \;+\mathcal{O}\left((a_1 p_{\text{max}})^{-3}\right) \;=\; -0.75\,\pi\;.
\end{aligned} \tag{5.23}$$

The bulk solutions are plotted for various values of $p_{\max}$ in Fig. (16). The closer the scattering length is to unitarity, the smaller the error. Conversely, natural values of the scattering lengths incur significant errors. For the solution of the trajectory equations that is in question, ϕ and θ maintain the conformal symmetry of the boundary solution, and therefore as long as the bulk data can reproduce the trajectory up to the fixed point of the conformal transformation, $p = 1/\sqrt{|a_0 a_1|} = 17.4$ MeV, the final segment of the curve can be obtained from the reflection isometry implied by the conformal invariance.

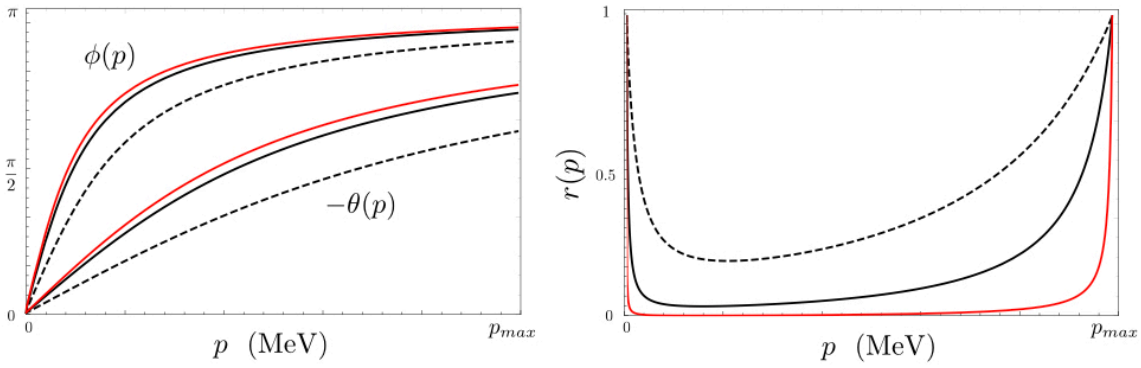

Figure 16. Bulk geodesics between S-matrix fixed points for LO in the ERE. The dashed (solid) black line corresponds to $p_{\max} = 50$ MeV (79 MeV). The red curve corresponds to $p_{\max} = 89$ MeV.

Thus, the potential in Eq. (5.18) has been engineered to provide a holographic dual of the nucleon-nucleon scattering matrix and, consequently, a kind of error-correcting code, where here "error" is in reference to violations of unitarity due to inelastic lossiness. The existence of $p_{\max}$ indicates that the elastic trajectory cannot be holographically reproduced for $p > p_{\max}$. Fig. (13) illustrates this particular error-correcting code.

6 Projections on $\mathbb{R}^2$ and $\mathbb{R}^3$

6.1 Non-conservative entanglement forces

The embedding of the unitarity surface in $\mathbb{R}^4$ gave rise, in the chosen coordinate system, to the flat torus, which allowed for a straightforward solution of the trajectory equations. However, the intrinsic four-dimensional nature of the space renders visualization difficult. In the original considerations of geometry, it was seen that a projection onto the (x, z) and (y, w) planes gave rise to a compact rhombus which the S-matrix trajectory is confined to by unitarity. Moreover, as will be seen below, the two unitarity constraints on the coordinates x, y, z, w can be used to describe a surface of constraint in three dimensions. How then does one describe these geometries?

Consider a subspace of the space described by the flat torus metric g_{ab} with line element

$$ds^2 \;=\; dx^2 \,+\, dy^2 \,+\, dz^2 \,+\, dw^2 \;=\; \tfrac{1}{2}\,\left(d\phi^2 \,+\, d\theta^2\right)\,. \tag{6.1}$$

The metric $\bar{g}_{ab}$ of the subspace is related to the flat torus metric via

$$g_{ab} \;=\; \bar{g}_{ab} \;+\; h_{ab} \;, \tag{6.2}$$

where h_{ab} describes the remainder subspace of the flat torus which is left out of the projection. With the assumption of conservative forces, the projected space is described by the trajectory equation

$$\ddot{\mathcal{X}}^a \;+\; {}_{\bar{g}}\Gamma^a{}_{bc}\dot{\mathcal{X}}^b\dot{\mathcal{X}}^c \;=\; \kappa(\sigma)\dot{\mathcal{X}}^a \;-\; \tfrac{1}{2}\mathbf{N}^2\bar{g}^{ab}\partial_b\bar{\mathbb{V}}(\mathcal{X}) \;, \tag{6.3}$$

where ${}_{\bar{g}}\Gamma^a{}_{bc}$ are the Christoffel symbols for the metric of the projected space $\bar{g}_{ab}$. It is straightforward to see that the assumption of conservative forces must be abandoned. Expressing the trajectory equation on the flat torus, Eq. (4.2), as

$$\ddot{\mathcal{X}}^a \;+\; g^{ad}{}_g\Gamma_{dbc}\dot{\mathcal{X}}^b\dot{\mathcal{X}}^c \;=\; \kappa(\sigma)\dot{\mathcal{X}}^a \;-\; \tfrac{1}{2}\mathbf{N}^2 g^{ab}\partial_b\mathbb{V}(\mathcal{X}) \;, \tag{6.4}$$

and noting that

$${}_g\Gamma_{dbc} \;=\; {}_{\bar{g}}\Gamma_{dbc} \;+\; {}_h\Gamma_{dbc} \quad , \quad \bar{g}_{ab}g^{bc} = 2\bar{g}_a{}^c \tag{6.5}$$

it is straightforward to recover Eq. (6.3) but with the substitution

$$\partial_a\bar{\mathbb{V}} \;\to\; 2\bar{g}_a{}^b\partial_b\mathbb{V} \;-\; \frac{2}{\mathbf{N}^2}\,{}_{\bar{g}}\Gamma_{abc}\dot{\mathcal{X}}^b\dot{\mathcal{X}}^c \;. \tag{6.6}$$

Therefore, in the projected space, the entanglement force found in the original flat space is rescaled by the projected metric and in addition acquires a non-conservative component which exactly cancels the curvature component in the projected space. These arguments formalize the observation that the flat torus solution fixes the trajectories in various projections of the flat torus. However, the manner in which the trajectory equations arise in the projections will vary in that external forces and curvature effects may interchange their roles.

6.2 Embedding in $\mathbb{R}^2$

Consider the geometry of the rhombus. Here the S-matrix may be viewed in $\mathbb{R}^4$ as $\mathbb{S}_R \otimes \mathbb{R}^2$ with $\mathbb{S}_R$ denoting the rhombus. With the choice

$$ds^2 \;=\; ds_R^2 \;+\; dy^2 \;+\; dw^2 \quad , \quad ds_R^2 \;=\; dx^2 \;+\; dz^2 \tag{6.7}$$

the line element takes the form

$$ds_R^2 \;=\; \tfrac{1}{2}\,\sin^2\phi\,d\phi^2 \;+\; \tfrac{1}{2}\,\sin^2\theta\,d\theta^2 \;, \tag{6.8}$$

which gives the metric of the projected space:

$$\bar{g} = \tfrac{1}{2}\begin{pmatrix} \sin^2\phi & 0 \\ 0 & \sin^2\theta \end{pmatrix} \;. \tag{6.9}$$

Therefore, the remainder space is:

$$h = \tfrac{1}{2}\begin{pmatrix} \cos^2\phi & 0 \\ 0 & \cos^2\theta \end{pmatrix} \ . \tag{6.10}$$

The geodesic equations for an S-matrix trajectory with $\sigma = p$ are read off from Eq. (6.3) to be

$$\ddot{\phi} = \kappa(p)\dot{\phi} \ - \ (\dot{\phi})^2 \cot\phi \quad , \quad \ddot{\theta} \ = \ \kappa(p)\dot{\theta} \ - \ (\dot{\theta})^2 \cot\theta \ , \tag{6.11}$$

and the solutions are readily found. Including external forces, and making the substitution as in Eq. (6.6) immediately recovers the flat torus trajectory equations which give LO in the ERE (and the conformal range model). These solutions are plotted in the rhombi of Section 2.

6.3 Quartics and the squere

The constraint of Eq. (2.11) can be removed to give an equation for a quartic surface. Eliminating the w variable defines the x-y-z system:

$$y^2\left(x^2 \ + \ y^2 \ + \ z^2\right) \ + \ x^2 z^2 \ = \ y^2 \ . \tag{6.12}$$

This equation describes the compact object illustrated in Fig. (17) and Fig. (18), and which will be referred to as a "squere" because of its sphere-like and square-like properties[18]. The unit squere fits inside the unit sphere and has volume $8/3$. The S-matrix is a trajectory that is confined to the surface of the squere. The fixed points of the RG, given in Eq. (2.6) appear as four distinct points on the squere which lie on axes of symmetry. The regions of vanishing EP are found from Eq. (2.19) to be at $z = 0$ with $x^2 + y^2$ arbitrary, and at $x = y = 0$ with z arbitrary, giving rise to a circle and a line, both joining two fixed points, respectively. The fixed points and the non-entangling regions of the squere in the x-y-z system are shown in Fig. (17).

The symmetries of the constraint equations and the positions of the fixed points indicate that the z-w-x system (elimination of y) is equivalent to the x-y-z system. However, eliminating the x variable defines the y-z-w system, which is a distinct surface (see Fig. (18). Now two of the fixed points appear at the origin of coordinates (and the non-entangling regions are different). Again, the symmetries of the constraint equations and the positions of the fixed points indicate that the w-x-y system (elimination of z) is equivalent to the y-z-w system.

It is convenient to view the x-y-z (y-z-w) system as the surface on which the real (imaginary) part of the S-matrix lies. The nucleon-nucleon S-matrix at LO in the ERE is plotted on the squere in Fig. (17) (real part) and in Fig. (18) (imaginary part). The right-most panels illustrate how the rhombus, for instance Fig. (2), is just a particular two-dimensional cross-section of the squere.

[18] A parametric representation of the squere is realized by choosing any of the three coordinates in Eq. (2.16).

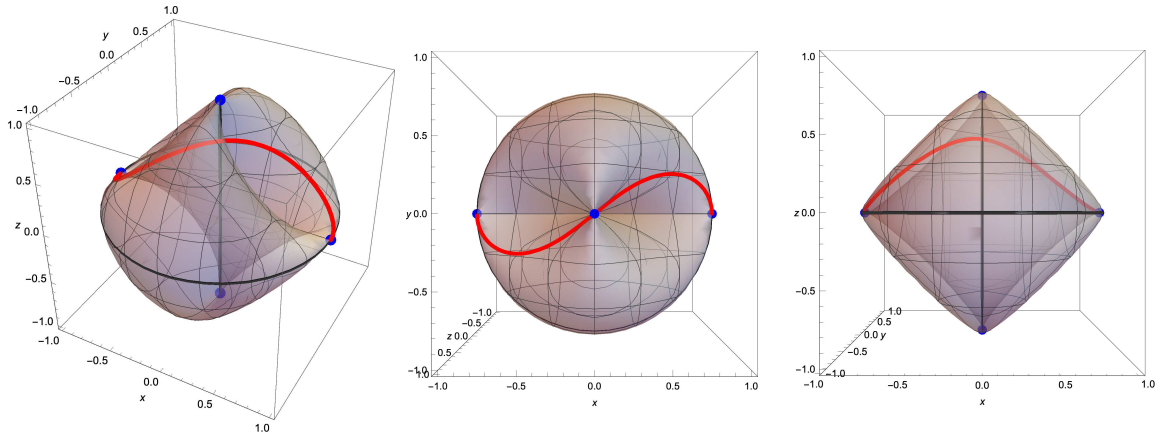

Figure 17. The squere in the x-y-z projection with several viewpoints of the real part of the S-matrix taken from LO in the ERE. The trajectory begins and ends at fixed points of the RG. The solid black lines are non-entangling geodesics.

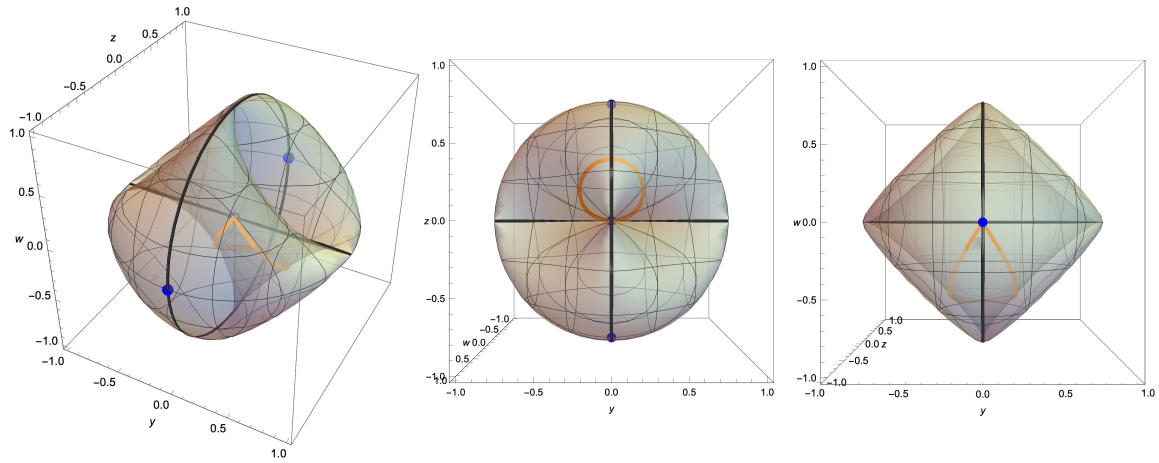

Figure 18. The squere in the y-z-w projection with several viewpoints of the imaginary part of the S-matrix taken from LO in the ERE. The trajectory begins and ends at fixed points of the RG. The solid black lines are non-entangling geodesics.

6.4 Embedding in $\mathbb{R}^3$

Metric and curvature

In order to study the geometry of the squere, the S-matrix may also be viewed in $\mathbb{R}^4$ as $\mathbb{S}_{\mathbb{Q}} \otimes \mathbb{R}$ with $\mathbb{S}_{\mathbb{Q}}$ denoting the squere. With the choice

$$ds^2 \;=\; ds_Q^2 \;+\; dw^2 \quad , \quad ds_Q^2 \;=\; dx^2 \;+\; dy^2 \;+\; dz^2 \tag{6.13}$$

the squere metric takes the form

$$ds_Q^2 \;=\; \tfrac{1}{4}\, r^2 \left(1 + \sin^2\phi\right) d\phi^2 \;+\; \tfrac{1}{4}\, r^2 \left(1 + \sin^2\theta\right) d\theta^2 \;+\; \tfrac{1}{2}\, r^2 \cos\phi \cos\theta \; d\phi \; d\theta \; . \tag{6.14}$$

The squere is an Einstein manifold with scalar curvature

$$R \;=\; \frac{32}{r^2}\frac{\sin\phi\sin\theta}{(-2+\cos 2\phi + cos2\theta)^2}\;, \tag{6.15}$$

and vanishing Einstein tensor

$$G_{ab} \;=\; R_{ab} \;-\; \tfrac{1}{2}R\,g_{ab} \;=\; 0\;. \tag{6.16}$$

The geodesic equations for an S-matrix trajectory with $\sigma = p$ are again read off from Eq. (6.3) to be

$$\begin{aligned}
\ddot{\phi} &= \kappa(\sigma)\,\dot{\phi} - \frac{2\cos\phi}{(-2+\cos 2\phi+\cos 2\theta)}\left[-(\dot{\phi})^2\sin\phi \;+\; (\dot{\theta})^2\sin\theta\right]\;,\\
\ddot{\theta} &= \kappa(\sigma)\,\dot{\theta} - \frac{2\cos\theta}{(-2+\cos 2\phi+\cos 2\theta)}\left[(\dot{\phi})^2\sin\phi \;-\; (\dot{\theta})^2\sin\theta\right]\;.
\end{aligned} \tag{6.17}$$

and the solutions are readily found. Including external forces, and making the substitution as in Eq. (6.6) immediately recovers the flat torus trajectory equations which give LO in the ERE (and the conformal range model). Both non-entangling geodesics and LO in the ERE are plotted in Fig. (17) and Fig. (18).

7 Summary and discussion

The ERE is a parameterization of the S-matrix which follows from the assumption that $p\cot\delta(p)$ is an analytic function in p^2. It is straightforward to derive the ERE using an EFT of contact operators which naturally gives rise to a momentum expansion. While the EFT is highly singular, and therefore the operator coefficients in the EFT are renormalization scheme and scale dependent, the ordering of operators provides a systematic expansion and the resulting S-matrix is physical and matches perfectly to the ERE. However, while EFT distinguishes between spin-entangling and non-spin-entangling interactions, and even reveals interesting patterns of symmetry, it does not provide much insight into the relative importance of these effects. Perhaps this is because the fundamental principle underlying EFT is locality in spacetime, and spin entanglement is intrinsically non-local. This motivates the search for a description of scattering that does not rely on an expansion in local operators. Treating the S-matrix as the fundamental object in the description of scattering suggests a spacetime-independent algorithm for generating the ERE in a manner in which entanglement is a purely geometrical property. In this paper, such a geometrical theory of scattering has been obtained.

The main results and observations regarding the geometrical S-matrix theory are:

• The S-matrix which describes low-energy nucleon-nucleon scattering has symmetries that are not visible in the EFT action. This observation, in itself, suggests that it is fruitful to view the S-matrix as a fundamental object, in some sense divorced from an EFT action. The

symmetries of the S-matrix involve inversions of the momenta, which interchange the UV and IR, and leave linear combinations of phase shifts invariant. As such it is not surprising that EFT is blind to these symmetries, since EFT is by construction an IR description of the S-matrix.

• The conformal UV/IR symmetries of the S-matrix are realized as orientation reversing isometries on a compact geometric space that is defined by unitarity. There is freedom in the choice of coordinates that describes this space. However, isotropy constraints are restrictive, and a geometric embedding in four-dimensional Euclidean space leads to a (two-dimensional) flat torus. The S-matrix corresponds to a curve which lives on this manifold and moves between RG fixed points.

• S-matrix trajectories with vanishing entanglement are special geodesics on the flat torus. In particular, in the absence of entanglement, the bulk of the flat torus becomes inaccessible and S-matrix trajectories evolve on a lattice with fixed points at the vertices and special geodesics as links between the vertices. In the absence of entanglement, the flat torus manifold does not exist.

Requiring the phase shifts to vanish at threshold uniquely picks out the non-entangling trajectory which moves along the central diagonal in Fig. (8). In nucleon-nucleon scattering this trajectory realizes an emergent $SU(4)$ spin-flavor symmetry of the effective action.

• Non-geodesic S-matrix trajectories on the flat torus that entangle spins are driven by an external entangling potential which permeates the flat torus and modifies the geodesic equations. The resulting equations are integrable when the S-matrix possesses the UV/IR conformal symmetry. This symmetry allows the explicit construction of the potential, which is a harmonic function on the flat torus.

• In contrast to EFT where the momentum expansion emerges as a consequence of locality of the interaction, the momentum variable in the geometric S-matrix formulation arises as a specific choice of inaffine parameterization of the geodesic equations. The forces that enter the trajectory equations are complicated non-local functions of the momentum, as one might expect in a spacetime-independent formulation of scattering.

• In the geometric formulation of scattering, inelasticity –a non-local effect in the EFT— is in correspondence with the radius of a three-dimensional hyperbolic space whose two-dimensional boundary is the flat torus. This space has a singularity at vanishing radius, corresponding to maximal violation of unitarity and vanishing EP. The boundary trajectory can be explicitly constructed from a bulk trajectory with a quantifiable error, providing a simple example of holographic duality and quantum error correction [36, 37]. It may be feasible to design more intricate bulk trajectories that reproduce boundary properties with smaller errors.

The holographic construction of S-matrix theory provides a forum for the consideration of fundamental questions. In the AdS/CFT correspondence [38], the conformal field theory on the boundary is a unitary theory and therefore the holographic correspondence suggests that all bulk properties are consistent with unitary evolution. In the simple hologram constructed in this paper, the boundary space is not simply a flat space on which an S-matrix propagates via unitary evolution, rather the theory space is in some sense "unitarity itself" as the space is defined by the constraints which enforce the unitarity of the S-matrix. Of course there is no time and consequently no causality[19] in the geometric S-matrix description and therefore implications for quantum gravity and spacetime in general are unclear.

A motivation for pursuing a formulation of scattering that does not rely on spacetime locality is to obtain new insight regarding the hierarchy of entangling operators that is observed in EFT. In this respect, the results of this study are mixed. While the assumption of finite and equal values of the two scattering lengths implies Wigner's $SU(4)$ spin-flavor symmetry in the EFT action, in the geometric construction, equal values of the scattering lengths constrains S-matrix trajectories to lie on geodesics that connect fixed points. There is therefore enhanced discrete symmetry on the flat torus when the scattering lengths are equal —*i.e.* $\phi = \theta$— and the S-matrix trajectory lies on a non-entangling geodesic. However, on the flat torus there is also enhanced discrete symmetry when $\phi = -\theta$ and the trajectory lies on an entangling trajectory. This asymmetry of entanglement reflects the entanglement power's preferred direction on the flat torus: lines of equi-entanglement are always parallel to $\phi = \theta$. The flat-torus construction does not seem to provide any insight into the origin of this asymmetry.

A more-specialized motivation of this new formulation of scattering theory is to learn about mysterious aspects of the nucleon-nucleon EFT construction that emerge as soon as the pion is included as a fundamental degree of freedom[20]. The pion interactions give rise to a tensor force in spin-triplet channels which wreaks havoc on the original EFT construction formulated in Ref. [14, 40]. For instance, in the chiral limit, the ${}^3S_1$ interaction is governed by an attractive $1/r^3$ potential whose singular nature has confounded attempts to provide a compelling regularization and renormalization scheme which would allow a description of nucleon-nucleon interactions within a single, unified, and systematic framework [41–46]. Here the focus has been on understanding the geometric S-matrix theory of delta-function interactions. A natural generalization would be to consider non-relativistic systems with other varieties of singular potentials. It may be that the geometric construction, which does not make an *a priori* separation between short- and long-distance effects, provides insight regarding the renormalization of the nucleon-nucleon EFT relevant at energies where the pion should be included as a fundamental degree of freedom.

One may wonder about the generality of the geometric S-matrix construction, and in particular whether some general underlying conditions that give rise to such a description can

[19] In some sense, causality does constrain S-matrix trajectories as effective range corrections are restricted via the Wigner bound [29–31].

[20] For a recent review, see Ref. [39]

be specified. Given the emphasis on the low-energy nucleon-nucleon system and the expression of the S-matrix as four-by-four matrices in the outer-product spin space of the two scattering nucleons, it may seem that this construction relies in some way on spin. However, even in the nucleon-nucleon system the construction does not rely on spin; *a priori* the nucleon-nucleon system appears symmetric under interchange of spin and isospin and it is only via the choice of spin basis that one speaks of spin entanglement. Presumably a choice of basis which emphasizes isospin and of course leaves the S-matrix unchanged would lead instead to isospin entanglement[21]. A simple condition which evidently should be satisfied in order to obtain a useful geometric formulation is that the codimension of the S-matrix trajectory in the space of all possible trajectories consistent with unitarity must be greater than or equal to one. So, for instance, the single-channel case with codimension-zero has no useful geometric description, whereas the nucleon-nucleon s-wave with codimension-one has a rich geometric representation. Other scattering systems and interactions with more than two bodies may provide further insight regarding this question.

Acknowledgments

We would like to thank Zohreh Davoudi, David B. Kaplan, Natalie Klco, Martin J. Savage, and Hersh Singh for important discussions. This work was supported by the U. S. Department of Energy grants **DE-FG02-97ER-41014** (UW Nuclear Theory) and **DE-SC0020970** (InQubator for Quantum Simulation).

References

[1] S. Weinberg, *Phenomenological Lagrangians*, *Physica A* **96** (1979), no. 1-2 327–340.

[2] K. Wilson and J. B. Kogut, *The Renormalization group and the epsilon expansion*, *Phys. Rept.* **12** (1974) 75–199.

[3] K. Audenaert, J. Eisert, M. Plenio, and R. Werner, *Entanglement Properties of the Harmonic Chain*, *Phys. Rev. A* **66** (2002), no. 4 042327, [quant-ph/0205025].

[4] S. Marcovitch, A. Retzker, M. Plenio, and B. Reznik, *Critical and noncritical long-range entanglement in Klein-Gordon fields*, *Phys. Rev. A* **80** (2009), no. 1 012325, [arXiv:0811.1288].

[5] P. Calabrese, J. Cardy, and E. Tonni, *Entanglement negativity in quantum field theory*, *Phys. Rev. Lett.* **109** (2012) 130502, [arXiv:1206.3092].

[6] N. Klco and M. J. Savage, *Geometric Quantum Information Structure in Quantum Fields and their Lattice Simulation*, arXiv:2008.03647.

[7] N. Arkani-Hamed, M. Pate, A.-M. Raclariu, and A. Strominger, *Celestial Amplitudes from UV to IR*, arXiv:2012.04208.

[8] N. Arkani-Hamed, S. He, G. Salvatori, and H. Thomas, *Causal Diamonds, Cluster Polytopes and Scattering Amplitudes*, arXiv:1912.12948.

[21] In the EFT, this is made manifest by Fierz transformation of the four-nucleon operators.

[9] N. Arkani-Hamed and P. Benincasa, *On the Emergence of Lorentz Invariance and Unitarity from the Scattering Facet of Cosmological Polytopes*, arXiv:1811.01125.

[10] D. B. Kaplan, M. J. Savage, and M. B. Wise, *A New expansion for nucleon-nucleon interactions*, *Phys. Lett.* **B424** (1998) 390–396, [nucl-th/9801034].

[11] D. B. Kaplan, M. J. Savage, and M. B. Wise, *Two nucleon systems from effective field theory*, *Nucl. Phys.* **B534** (1998) 329–355, [nucl-th/9802075].

[12] U. van Kolck, *Effective field theory of short range forces*, *Nucl. Phys.* **A645** (1999) 273–302, [nucl-th/9808007].

[13] M. C. Birse, J. A. McGovern, and K. G. Richardson, *A Renormalization group treatment of two-body scattering*, *Phys. Lett. B* **464** (1999) 169–176, [hep-ph/9807302].

[14] S. Weinberg, *Nuclear forces from chiral Lagrangians*, *Phys. Lett.* **B251** (1990) 288–292.

[15] S. R. Beane, D. B. Kaplan, N. Klco, and M. J. Savage, *Entanglement Suppression and Emergent Symmetries of Strong Interactions*, *Phys. Rev. Lett.* **122** (2019), no. 10 102001, [arXiv:1812.03138].

[16] T. Mehen, I. W. Stewart, and M. B. Wise, *Wigner symmetry in the limit of large scattering lengths*, *Phys. Rev. Lett.* **83** (1999) 931–934, [hep-ph/9902370].

[17] T. Mehen, I. W. Stewart, and M. B. Wise, *Conformal invariance for nonrelativistic field theory*, *Phys. Lett. B* **474** (2000) 145–152, [hep-th/9910025].

[18] U. van Kolck, *Unitarity and discrete scale invariance*, *Few-Body Systems* **58** (2017), no. 3 112.

[19] N. L. Harshman, *Dynamical entanglement in particle scattering*, *International Journal of Modern Physics A* **20** (Oct, 2005) 6220–6228.

[20] P. Zanardi, *Entanglement of quantum evolutions*, *Phys. Rev. A* **63** (Mar, 2001) 040304.

[21] A. D. Ballard and Y.-S. Wu, *Cross Disciplinary Advances in Quantum Computing*, ch. Cartan Decomposition and Entangleing Power of Braiding Quantum Gates. Contemporary mathematics - American Mathematical Society. American Mathematical Society, 2011.

[22] R. U. Nijmegen, "Nn-online." http://nn-online.org/, 2005. Accessed: 2018-12-01.

[23] E. Wigner, *On the Consequences of the Symmetry of the Nuclear Hamiltonian on the Spectroscopy of Nuclei*, *Phys. Rev.* **51** (1937) 106–119.

[24] E. Wigner, *On the Structure of Nuclei Beyond Oxygen*, *Phys. Rev.* **51** (1937) 947–958.

[25] E. P. Wigner, *On Coupling Conditions in Light Nuclei and the Lifetimes of beta-Radioactivities*, *Phys. Rev.* **56** (1939) 519–527.

[26] D. B. Kaplan and M. J. Savage, *The Spin flavor dependence of nuclear forces from large n QCD*, *Phys. Lett.* **B365** (1996) 244–251, [hep-ph/9509371].

[27] D. B. Kaplan and A. V. Manohar, *The Nucleon-nucleon potential in the 1/N(c) expansion*, *Phys. Rev.* **C56** (1997) 76–83, [nucl-th/9612021].

[28] A. Calle Cordon and E. Ruiz Arriola, *Wigner symmetry, Large N(c) and Renormalized One Boson Exchange Potential*, *Phys. Rev.* **C78** (2008) 054002, [arXiv:0807.2918].

[29] E. P. Wigner, *Lower Limit for the Energy Derivative of the Scattering Phase Shift*, *Phys. Rev.*

98 (1955) 145–147.

[30] D. R. Phillips and T. D. Cohen, *How short is too short? Constraining contact interactions in nucleon-nucleon scattering*, *Phys. Lett. B* **390** (1997) 7–12, [nucl-th/9607048].

[31] H.-W. Hammer and D. Lee, *Causality and the effective range expansion*, *Annals Phys.* **325** (2010) 2212–2233, [arXiv:1002.4603].

[32] I. Bengtsson and K. Zyczkowski, *Geometry of Quantum States: An Introduction to Quantum Entanglement*. Cambridge University Press, 2006.

[33] I. Bengtsson, J. Brännlund, and K. Życzkowski, *Cpn, or, entanglement illustrated*, *International Journal of Modern Physics A* **17** (Dec, 2002) 4675–4695.

[34] I. Garay and S. Robles-Pérez, *Classical geodesics from the canonical quantisation of spacetime coordinates*, arXiv:1901.05171.

[35] M. Blau, *Lecture notes on general relativity*, 2020. http://www.blau.itp.unibe.ch/GRLecturenotes.html.

[36] A. Almheiri, X. Dong, and D. Harlow, *Bulk Locality and Quantum Error Correction in AdS/CFT*, *JHEP* **04** (2015) 163, [arXiv:1411.7041].

[37] F. Pastawski, B. Yoshida, D. Harlow, and J. Preskill, *Holographic quantum error-correcting codes: Toy models for the bulk/boundary correspondence*, *JHEP* **06** (2015) 149, [arXiv:1503.06237].

[38] J. M. Maldacena, *The Large N limit of superconformal field theories and supergravity*, *Int. J. Theor. Phys.* **38** (1999) 1113–1133, [hep-th/9711200].

[39] U. van Kolck, *The Problem of Renormalization of Chiral Nuclear Forces*, *Front. in Phys.* **8** (2020) 79, [arXiv:2003.06721].

[40] S. Weinberg, *Effective chiral Lagrangians for nucleon - pion interactions and nuclear forces*, *Nucl. Phys. B* **363** (1991) 3–18.

[41] D. B. Kaplan, M. J. Savage, and M. B. Wise, *Nucleon - nucleon scattering from effective field theory*, *Nucl. Phys. B* **478** (1996) 629–659, [nucl-th/9605002].

[42] S. Fleming, T. Mehen, and I. W. Stewart, *NNLO corrections to nucleon-nucleon scattering and perturbative pions*, *Nucl. Phys. A* **677** (2000) 313–366, [nucl-th/9911001].

[43] S. R. Beane, P. F. Bedaque, M. J. Savage, and U. van Kolck, *Towards a perturbative theory of nuclear forces*, *Nucl. Phys. A* **700** (2002) 377–402, [nucl-th/0104030].

[44] A. Nogga, R. Timmermans, and U. van Kolck, *Renormalization of one-pion exchange and power counting*, *Phys. Rev. C* **72** (2005) 054006, [nucl-th/0506005].

[45] M. C. Birse, *Power counting with one-pion exchange*, *Phys. Rev. C* **74** (Jul, 2006) 014003.

[46] D. B. Kaplan, *Convergence of nuclear effective field theory with perturbative pions*, *Phys. Rev. C* **102** (2020), no. 3 034004, [arXiv:1905.07485].